Science of the Total Environment 901 (2023) 166376

Contents lists available at ScienceDirect

Science of the Total Environment

journal homepage: www.elsevier.com/locate/scitotenv

Efficient and sustainable photocatalytic inactivation of *E. coli* by an innovative immobilized Ag/TiO_2 photocatalyst with peroxymonosulfate (PMS) under visible light

Jialin Jia [a,b], Stefanos Giannakis [c,*], Dong Li [d], Boyin Yan [a], Tao Lin [a,b,*]

[a] Ministry of Education Key Laboratory of Integrated Regulation and Resource Development on Shallow Lakes, Hohai University, Nanjing 210098, PR China
[b] College of Environment, Hohai University, Nanjing 210098, PR China
[c] Universidad Politécnica de Madrid, E.T.S. de Ingenieros de Caminos, Canales y Puertos, Departamento de Ingeniería Civil: Hidráulica, Energía y Medio Ambiente, Environment, Coast and Ocean Research Laboratory (ECOREL-UPM), c/ Profesor Aranguren, 3, ES-28040, Madrid, Spain
[d] Collaborative Innovation Center of Atmospheric Environment and Equipment Technology, Jiangsu Key Laboratory of Atmospheric Environment Monitoring and Pollution Control, School of Environmental Science and Engineering, Nanjing University of Information Science & Technology, Nanjing 210044, PR China

HIGHLIGHTS

- SCA made Ag nanoparticles firmly and evenly dispersed on TiO_2NTAs.
- Ag/SCA/TiO_2NTAs showed effective inactivation combined with PMS under visible light (VL) irradiation.
- Ag/SCA/TiO_2NTAs/PMS/VL system exhibited excellent stability and reusability compared to similar systems.
- SCA played a pivotal role in the production of reactive species.
- Ag/SCA/TiO_2NTAs/PMS/VL system has a good inactivation performance in tap water and matrices mimicking natural waters.

GRAPHICAL ABSTRACT

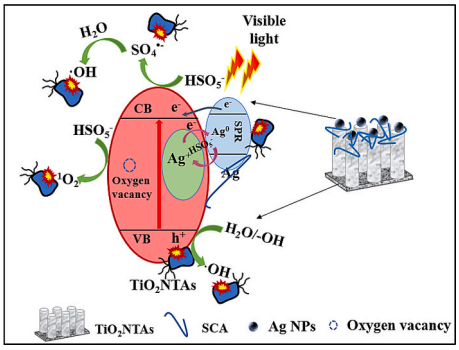

ARTICLE INFO

Editor: Kyle Bibby

Keywords:
TiO_2 photocatalysis
Ag nanoparticles
Silane coupling agent
Peroxymonosulfate
E. coli inactivation

ABSTRACT

A novel catalytic system for effective photocatalytic inactivation of *Escherichia coli* (*E. coli*) was constructed by anchoring Ag nanoparticles (AgNPs) on silane coupling agent (SCA) pretreated TiO_2 nano-tube arrays (Ag/SCA/TiO_2NTAs). Morphology and structural analyses revealed that SCA could disperse AgNPs evenly on TiO_2NTAs, thus inducing a superior surface plasmon resonance (SPR) effect. Ag/SCA/TiO_2NTAs catalyst exhibited excellent inactivation performance when in the presence of peroxymonosulfate (PMS) and visible light (VL), with 6-log *E. coli* was completely inactivated within 60 min, which was 5.3, 12.5 and 13.2 times higher than that of Ag/SCA/TiO_2NTAs/VL, PMS/VL and Ag/SCA/TiO_2NTAs/PMS/dark systems, respectively. Additionally, the photocatalyst exhibited a highly reusable property, with the inactivation performance almost unchanged after ten cycles of uses with minimal Ag leaching. The inactivation mechanism analysis demonstrated that both radical ($SO_4^{\bullet-}$, $^{\bullet}OH$) and non-radical (h^+, $^1O_2$) pathways involved in *E. coli* inactivation, and SCA played a pivotal role in the production of reactive species. Chloride ions (Cl^-) greatly enhanced the inactivation efficiency, while bicarbonate (HCO_3^-) and phosphate ($H_2PO_4^-$) showed an inhibitory effect. Humic acid (HA) displayed a dual effect

* Corresponding authors.
E-mail addresses: stefanos.giannakis@upm.es (S. Giannakis), 20040076@hhu.edu.cn (T. Lin).

https://doi.org/10.1016/j.scitotenv.2023.166376
Received 19 January 2023; Received in revised form 10 August 2023; Accepted 15 August 2023
Available online 16 August 2023

on inactivation performance, where the low concentration of HA facilitated the bacteria inactivation, while the higher dose suppressed bacteria inactivation. Moreover, the system exhibited excellent inactivation performance in tap water. This work first used SCA as the binder to fix AgNPs on TiO_2NTAs for VL photocatalytic inactivation of bacteria with the assistance of PMS, which was expected to provide some insights into the practical treatment of drinking water.

1. Introduction

Despite the great advances in sanitation and water distribution, pathogenic microorganisms in drinking water still constitute a valid reason for concern for treatment plant operators, since they can cause some water-borne diseases such as polio, cholera, and diarrhea (López-Vinent et al., 2022), these pose a serious threat to public health and impede societal and economic development. Among various pathogens, *Escherichia coli* (*E. coli*) is one of the most common diarrhea-causing bacteria, it has been reported that over 80,000 people die from diarrhea each year (López-Vinent et al., 2022; Rodríguez-Chueca et al., 2019). In addition, *E. coli* may also provoke thrombotic thrombocytopenic purpura, hemolytic uremic syndrome, and urinary tract infections (Zottola and Smith, 1990). Ozonation and chlorination are efficient for water disinfection, but their practical application is still under caution, partially due to the high cost but mainly due to the hazardous disinfection by-products (DBPs) generated (Chen et al., 2022; Zheng et al., 2023). Therefore, there is an urgent need to develop an alternative technique for effective disinfection in water.

Photocatalytic disinfection has been considered an alternative promising technology for small-scale plants, not only because it can use solar energy, but also due to the sustainable use of some photocatalysts, and can avoid the generation of toxic and harmful DBPs (Sayılkan et al., 2009; Chen et al., 2023). Titanium dioxide (TiO_2) is the most commonly used photocatalyst thanks to its non-toxicity, chemical stability and low cost (Andersson et al., 2002). However, its photocatalytic efficiency, especially in visible light (VL) is usually unsatisfactory due to the wide band gap energy (3.2 eV) and rapid recombination of photo-generated carriers (Srinivasan et al., 2006). To address this issue, many attempts have been conducted such as its coupling with narrow-band semiconductors, doping with metal/non-metals, heterojunctions, or decoration of noble metals on its surface. Owing to the surface plasmon resonance (SPR) effect, noble metal modification can greatly enhance the photocatalytic activity of TiO_2 since the noble metal could trap the photogenerated electrons to decrease the recombination rate of photo-induced electron-hole pairs (Wang et al., 2017). Among several noble metals, Ag costs significantly less, and Ag itself is also a material with a known disinfecting capacity (Kohantorabi et al., 2021a). Many studies had combined Ag and TiO_2 for the inactivation of *E. coli* in water. For instance, Hajjaji et al. (2018) used an Ag-decorated TiO_2-nanotubes photocatalyst to activate *E. coli* under VL irradiation, results revealed that 6-log of *E. coli* could be completely inactivated within 90 min. Wang and Lim (2013) synthesized Ag-AgBr/TiO_2 photocatalyst and found that the prepared photocatalyst exhibited much better photocatalytic activity than that of bare TiO_2 in white LED, which could achieve 7-log *E. coli* inactivation within 60 min.

Although these studies have achieved good disinfection results, some aspects of this technique still need to be addressed and improved, specifically: (1) the difficulties in separation and recovery of powder photocatalysts after disinfection is still a key point that constrains the photocatalytic disinfection applied in large-scale industry, (2) AgNPs usually aggregate easily and leach seriously, which is another factor restricting its practical application, (3) the photocatalytic disinfection efficiency in VL needs to be further improved.

For the first two issues, the combination of suitable materials and methods to synthesize immobilized catalysts is almost a one-way road (Ho et al., 2019). Solid matrices like cellulose (Zeng et al., 2010), clay (Bel Hadjltaief et al., 2016), and cement (Delnavaz et al., 2015) have been employed to construct immobilized catalysts. However, most of these catalysts are restricted by the complex preparation process and hazardous chemicals involved in the synthesis. Taking that into account, selecting immobilized TiO_2 (Ti plate or Ti mesh) is feasible since it can be used as the catalyst carrier and the photocatalyst simultaneously. Besides, based on previous reports, the silane coupling agents (SCAs) can be selected as the binder because of their strong "bridging" effect, and the hydrophobicity of SCAs can make the catalyst more evenly dispersed (Sang et al., 2017). For the third issue, introducing oxidants, such as persulfate (PDS), peroxymonosulfate (PMS), and hydrogen peroxide (H_2O_2) into the photocatalytic process can greatly improve the photocatalytic capacity since the oxidant can induce the production of further series of reactive species. Among the various oxidants used so far, PMS has attracted much attention because of its high oxidation capacity (Giannakis et al., 2021), chemical stability (Anipsitakis and Dionysiou, 2003), and easy activation in catalytic processes (Kohantorabi et al., 2021b). These properties have led to its wide testing for the elimination of various organic pollutants, as well as the inactivation of bacteria and viruses (López-Vinent et al., 2022; Marjanovic et al., 2018; Rodríguez-Chueca et al., 2019).

To the best of our knowledge, so far there is no report employing SCAs for Ag/TiO_2 photocatalyst immobilization with subsequent activation of PMS under VL irradiation for water disinfection. Based on the above discussion and the advantages the proposed combination may bring, in this study, according to a simple method we attempt to prepare a TiO_2-based immobilized photocatalyst, operational in VL, for PMS-mediated advanced water treatment. Specifically, TiO_2 nanotube arrays (TiO_2NTAs) were prepared by anodic oxidation of Ti mesh at room temperature, while SCAs and the photoreduction deposition method were subsequently used to anchor AgNPs on the TiO_2NTAs. The physicochemical, electronic, and structural stability properties of the catalyst were studied systematically by a series of characterization techniques, and the bacterial inactivation performance of the catalyst after activating PMS under VL irradiation was evaluated with *E. coli* as the model pathogen. The insights on the probable inactivation mechanism were provided by conducting appropriate quenching experiments coupled with Electron Paramagnetic Resonance (EPR) tests. The influences of inorganic anions and natural organic matter (NOM) on inactivation performance were also evaluated to assess the robustness of the system to the water composition. Furthermore, the inactivation in tap water was also conducted to investigate the practical suitability of the system.

2. Materials and methods

2.1. Chemicals and reagents

Titanium mesh (80 mesh, 99.8 % purity) was purchased from Kang Wei Metal Screen Products Co., Ltd. (Hebei, China). Silver nitrate ($AgNO_3$; Sinopharm, China), 3-(Methacryloyloxy) propyltrimethoxysilane (KH570, a kind of SCAs; Aladdin, China). Peroxymonosulfate (Oxone, $2KHSO_5{\cdot}KHSO_4{\cdot}K_2SO_4$; Merk, Spain), Sodium bicarbonate ($NaHCO_3$; Merk, Spain), sodium chloride (NaCl; Merk, Spain), potassium phosphate (KH_2PO_4; Merk, Spain), humic acid (HA; Sigma-Aldrich, China). All the other chemicals and reagents were analytically pure without further purification. Milli-Q water was used throughout the experiments.

2.2. Preparation of immobilized Ag/TiO_2NTAs photocatalyst

The immobilized Ag/TiO_2NTAs photocatalyst was prepared by employing Ti mesh as the substrate since its three-dimensional grid structure can provide more active sites. Firstly, TiO_2NTAs were grown in situ on Ti mesh and were obtained by an anodization method, based on a previous study (Jia et al., 2020a). Then, the prepared TiO_2NTAs were put into a mixture of water and ethanol (the volume ratio is 1:1) with 0.25 g KH570 (a kind of SCA) in it. After stirring for 1 h at 80 °C, the modified TiO_2NTAs by KH570 was obtained after drying at 60 °C for 2 h. After that, the photoreduction method was employed to deposit Ag onto TiO_2NTAs by employing $AgNO_3$ as a precursor. Briefly, the pretreated TiO_2NTAs by KH570 were immersed into the $AgNO_3$ solution (50 mL, 0.01 mol/L) at 60 °C for 1 h. Then, a xenon lamp (300 W, full spectrum) was turned on, the entire photoreduction process lasted 1 h. After rinsing the sample several times with deionized water, the immobilized Ag/TiO_2NTAs photocatalyst was finally obtained after drying in an oven for 1 h at 60 °C, hereon which was denoted as Ag/SCA/TiO_2NTAs. The load amount of Ag was about 0.005 g by calculating the mass difference before and after above processing steps, the specific process was shown in Fig. 1. In addition, to highlight our research, comparative experiments were also conducted, where Ag was deposited directly on TiO_2NTAs without SCA treatment (the Ag load was about 0.009 g), denoted as Ag/TiO_2NTAs.

2.3. Characterization

The crystal structure of the photocatalysts was recorded by a Bruker D8 X-ray diffractometer (XRD) equipped with Cu Ka radiation (λ = 0.15418 nm). The surface morphology was observed by a field emission scanning electron microscope (FE-SEM, Zeiss SUPRA 55 SAPPHIRE). The optical properties of samples were analyzed by UV–vis diffuse reflectance spectra (DRS) (Shimadzu, UV2550). The surface chemistry states were investigated using X-ray photoelectron spectroscopy (XPS, ESCALAB 250, Thermo) with Al Kα line (1486.6 eV) radiation. The reactive species were identified by EPR (Bruker, A200, Germany).

2.4. Bacterial preparation protocol

As the most commonly used indicator of intestinal pathogens, *E. coli* K12, a non-pathogenic wild-type strain was selected as the model bacteria in disinfection experiments. *E. coli* was stored in cryo-vials containing 20 % glycerol at −80 °C. The detailed preparation protocol is provided elsewhere (Giannakis et al., 2022). In short, the inoculated LB medium was inoculated by an *E. coli* colony and was incubated overnight at 37 °C, with continuous shaking at 180 rpm, and then used for the preparation of the stock of stationary phase bacteria. 1 mL of the suspension was centrifuged at 8000 rpm for 2 min, followed by washing the bacterial pellet with sterile saline solution (0.8 g KCl/L, 8 g NaCl/L). The obtained bacterial stock was about 10^9 CFU/mL, then was further diluted to 10^6 CFU/mL, which was the experimental concentration.

2.5. Inactivation experiments and analytical methods

2.5.1. Bacterial inactivation experiments

All the inactivation experiments were performed in Milli-Q water with a certain amount of *E. coli* in it, where a 100 mL quartz cylinder was employed as the reactor with 50 mL bacterial suspension. The VL was emitted by an array of TLD-type lamps (Philips) with a light intensity of 93.5 ± 0.5 W/m^2, the emission spectrum (as per manufacturer) of the lamp is displayed in Fig. S1. The irradiated (available) area of the photocatalyst was 1 × 2 cm^2. The temperature of the reaction system did not exceed 30 °C. The inactivation experiment was triggered by adding a certain amount of PMS to the reaction system and light introduction to the system. At desired time intervals, 100 μL samples were taken from the reactor, immediately spread on Petri dishes containing plate count agar, or serially diluted (1:10) in saline solution to guarantee measurable counts of colonies when necessary. The *E. coli* colonies were manually counted after 24 h incubation at 37 °C.

2.5.2. Ag leaching experiments

The concentration of leached Ag in the reaction solution was measured on an ICP-MS spectrometer (Perkin Elmer, Optima 5300DV). Prior to the determination, the solution was sampled under constant stirring, and was filtered manually with the injection syringe equipped with a 0.22 um filter membrane. Then, 1 μL solution was diluted to 10 mL by using 3 % nitric acid matrix. A 5-point standard curve was made to evaluate the leached Ag ions concentration, with a range of 1–50 ppb (1, 5, 10, 20, 30 and 50 ppb prepared by volume) which was diluted in the 3 % nitric acid matrix. All standards and samples were measured for 3 times and averaged. A 30 s flush time with ultrapure water was conducted between all runs. Before the measurement of each unknown sample, two blanks were analyzed to verify removal of all residual metals from the instrument.

2.5.3. ROS exploration experiments

To explore the roles of reactive species generated in the system, certain amounts of radical quenchers like isopropanol (IPA), sodium

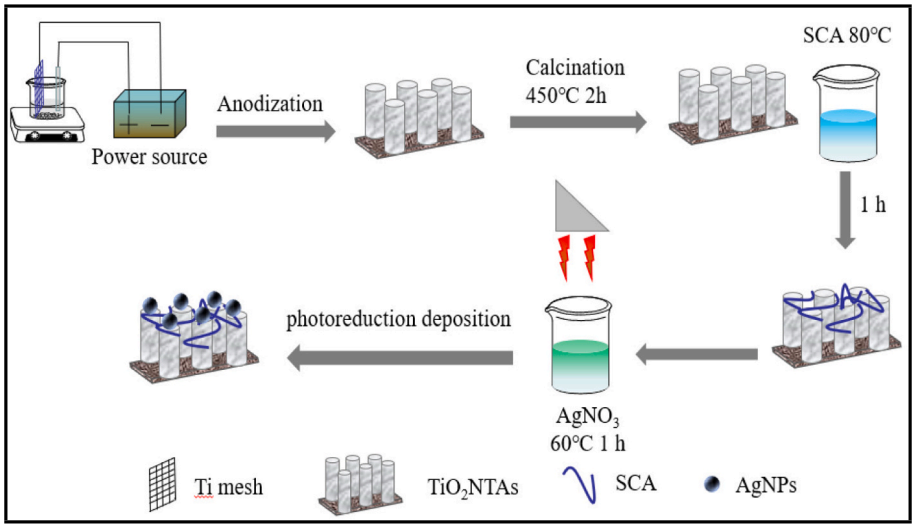

Fig. 1. Schematic diagram of Ag/SCA/TiO_2NTAs preparation process.

chloride (NaCl), sodium oxalate, superoxide dismutase (SOD), and L-histidine were added into the system to quench •OH, $SO_4^{\bullet-}$, h^+, $O_2^{\bullet-}$, $^1O_2$, respectively. For electron paramagnetic resonance (EPR) experiments, 5,5-dimethyl-1-pyrroline N-oxide (DMPO) and 2,2,6,6-Tetramethyl-4-piperidinol (TEMP) were employed as spin-trapping reagents for radicals and singlet oxygen ($^1O_2$) detection, respectively. The EPR spectra was recorded using a Bruker A200 spectrometer (Germany) under following conditions: microwave power = 18.7 mW, microwave frequency = 9.766 GHz, temperature = 20 °C.

2.5.4. Inactivation in matrices mimicking natural water bodies

The tests on bacteria inactivation efficacy of system in different water background composition were conducted by introducing a certain amount of NaCl, $NaHCO_3$, KH_2PO_4 and humic acid (HA) to the reaction system, and HA stock solutions were prepared based on our previous study (Jia et al., 2020a, 2020b).

All experiments were conducted in triplicate, and the average values with standard deviations were employed which denoted by error bars in corresponding graphs.

2.6. Statistical analysis

Analysis of variance (one-way ANOVA) was used to compare the effects of different concentrations of PMS and water matrix on *E. coli* inactivation at 60 min. In addition, student's *t*-test was used to statistically analyze the *E. coli* inactivation under different treatments and the Ag leaching of different systems at 60 min from the first use to the fourth use, and the results were returned to a *p* value. All *p* values <0.05 were considered statistically significant.

3. Results and discussion

3.1. Characterization of the photocatalyst

The morphologies of Ag/TiO_2NTAs and Ag/SCA/TiO_2NTAs were studied by SEM. As can be seen in Fig. 2, the particles scattered on the surface of TiO_2NTAs in the Ag/TiO_2NTAs sample are likely to be agglomerated AgNPs, and with further magnifying of the images, some cubic like crystals were found on the surface of TiO_2NTAs (Fig. 2a–b). Nevertheless, under the same magnification, no serious aggregates were found in Ag/SCA/TiO_2NTAs (Fig. 2c), instead, it was found that some small Ag pellets were distributed evenly along the edge of TiO_2NTAs or inside of it (Fig. 2d). To better highlight the effect of SCA, and the consistency of samples morphology, the SEM images at different regions of the samples were also taken. As shown in Fig. S5b–d, the particles are relatively uniform and monodisperse, having particles of approximately the same size, and no AgNPs agglomeration was found in Ag/SCA/TiO_2NTAs compared with Ag/TiO_2NTAs (Fig. S5a). The particle size distribution histogram of AgNPs of Ag/SCA/TiO_2NTAs was measured with nano-measurer software and the average size was 24 ± 5.3 nm (Fig. S6(a)), and the size range of AgNPs in Ag/TiO_2NTAs was 105–519 nm with the average size of 260 ± 65.1 nm (Figs. 2a and S6(b)). A previous study has reported that SCA (KH570) could stabilize and restrain nanoparticles aggregation by diminishing the -OH groups of nanoparticles (Fu et al., 2021). Therefore, it can be concluded that in this study, the introduction of SCA effectively inhibited the agglomeration of AgNPs and made them more uniformly dispersed on TiO_2NTAs.

Fig. 3a depicts the XRD spectra of the as-prepared photocatalysts. The peaks at $2\theta = 25.6°$ and 63.1° could be ascribed to (101) and (204)

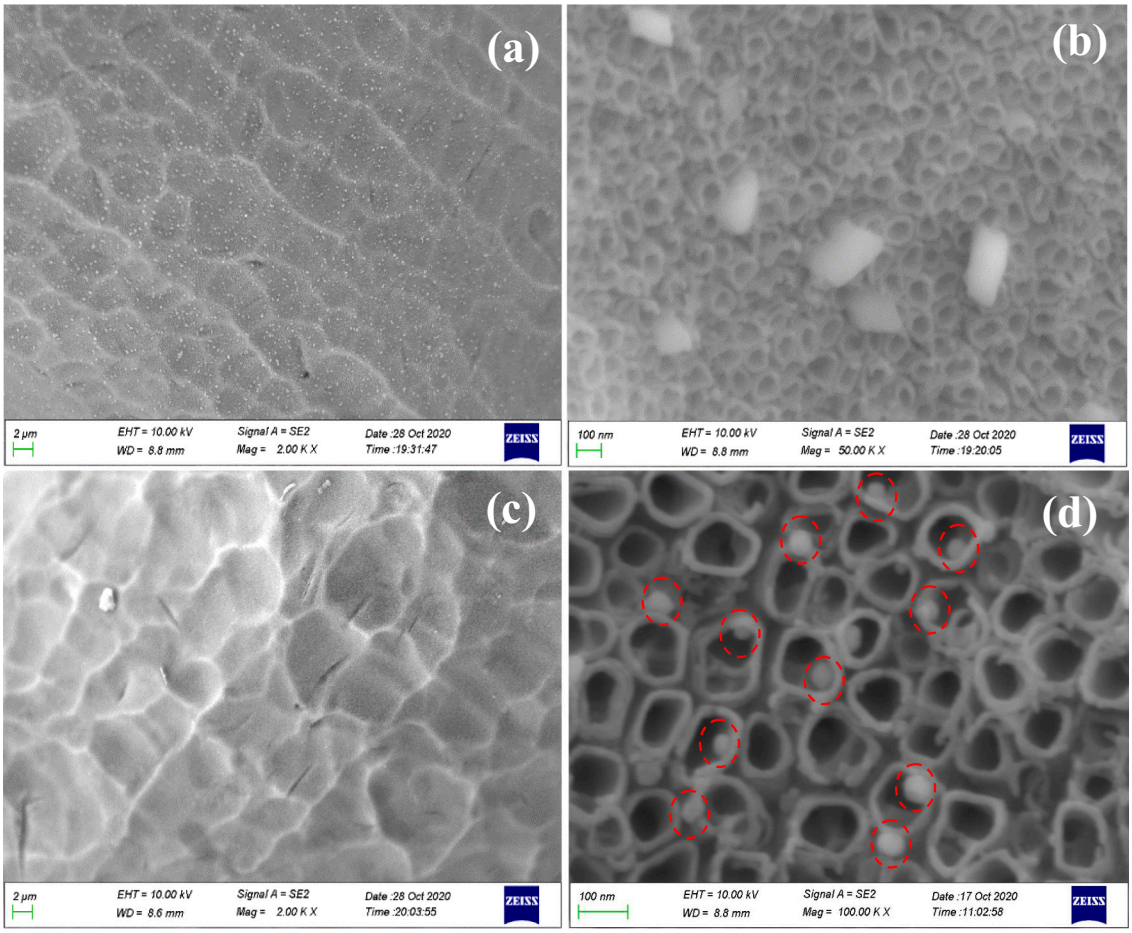

Fig. 2. SEM image of fresh Ag/TiO_2NTAs (a, b) and Ag/SCA/TiO_2NTAs (c, d).

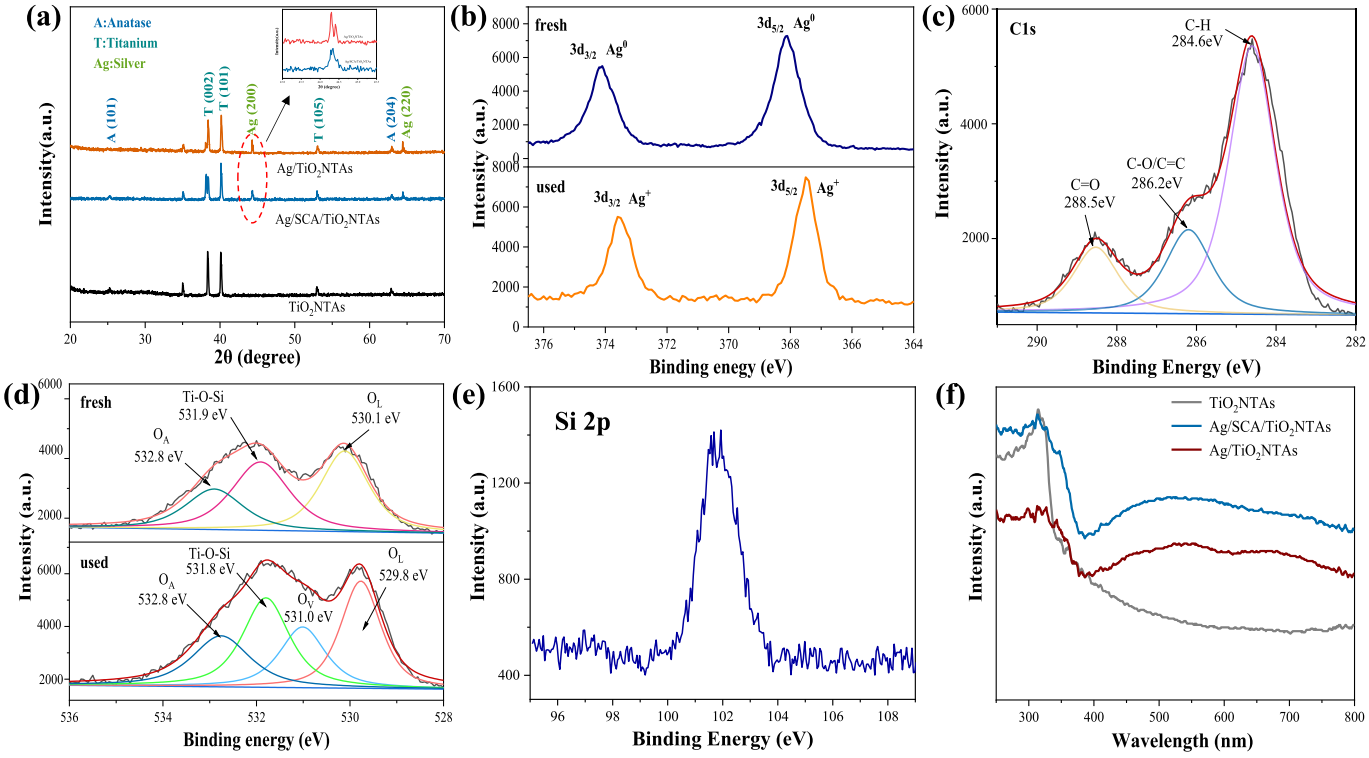

Fig. 3. XRD patterns of three fresh photocatalysts (a), high-resolution XPS spectra of Ag3d (b), C1s (c), O1s (d), Si2p (e) of fresh Ag/SCA/TiO_2NTAs, and UV–Vis DRS spectrum of three fresh photocatalysts (f).

planes of anatase phase TiO_2 (JCPDS NO. 21-1272), respectively (Li et al., 2021). Therefore, it can be confirmed that all three samples are crystallized in the anatase phase. Peaks at $2\theta = 38.3°$, 40.4°, and 53.1° were corresponding to (002), (101), and (105) crystal plane of Ti metal (JCPDS NO. 44-1294), respectively. In addition, peaks at $2\theta = 44.4°$ and 64.5° were observed both in Ag/TiO_2NTAs and Ag/SCA/TiO_2NTAs, which could be indexed to (200) and (220) planes of Ag^0, respectively (Chen et al., 2016). It should be noted that the characteristic peak of Ag in Ag/SCA/TiO_2NTAs was broader than that of Ag/TiO_2NTAs. According to Debye–Scherrer formula, the broader the half-peak width is, the smaller the particle size is. Namely, in this study, the particle size of Ag in Ag/SCA/TiO_2NTAs is smaller than that of Ag/TiO_2NTAs. The XRD analysis results were consistent with the SEM results, further indicating that the introduction of KH570 could suppress the agglomeration of AgNPs.

The elemental composition and electronic states of Ag/SCA/TiO_2NTAs constituents were analyzed by XPS. As shown in Fig. 3b, Ag 3d high-resolution XPS spectrum exhibited two peaks at 374.1 and 368.1 eV (Fig. 3b, fresh sample), which correspond to Ag 3d3/2 and Ag 3d5/2, respectively (indexed as Ag^0) (Wang et al., 2012). C1s spectrum consisted of three peaks (Fig. 3c), the peak at 284.6 eV could be ascribed to C—H and C—C (Ni et al., 2012). Peaks at 286.2 eV and 288.5 eV were C=C/C-O and C═O bonds, respectively (Zan et al., 2004), which could be due to the introduction of SCA. O 1 s spectrum (fresh sample) was divided into three peaks (Fig. 3d), the peak at 530.1 eV was the lattice oxygen of TiO_2 (Ji et al., 2016), the peak at 531.9 eV was assigned to the Ti-O-Si bond (Lu et al., 2000) and the peak at 532.9 eV was the -OH adsorbed on the surface of the photocatalyst (Ahmed et al., 2016). The characteristic peak of Si 2p was also found, however, its peak intensity was relatively weak compared to other peaks (Fig. 3e). XPS results suggested that the Ag element in the sample existed as metallic Ag^0, and SCA was successfully grafted onto TiO_2NTAs.

The optical property of the photocatalysts was explored by UV–vis DRS. As displayed in Fig. 3f, TiO_2NTAs showed strong absorption mainly in the ultraviolet region, while the absorption of Ag/TiO_2NTAs and Ag/SCA/TiO_2NTAs in the VL region (400–800 nm) was significantly stronger than that of TiO_2NTAs. The intense VL region absorption of Ag/TiO_2NTAs and Ag/SCA/TiO_2NTAs could be attributed to the SPR effect caused by Ag, which greatly enhanced the VL absorption of two photocatalysts. In addition, no matter in the ultraviolet region or VL region, the absorption intensity of Ag/SCA/TiO_2NTAs was always stronger than that of Ag/TiO_2NTAs. This could be ascribed to the fact that SCA made Ag more evenly dispersed on TiO_2NTAs for better VL absorption, while the weaker absorption of Ag/TiO_2NTAs was due to the higher agglomeration of AgNPs, which reduced the active sites of the photocatalyst, resulting in an inadequate SPR effect. Note that, although the peak broadness of Ag in both Ag/SCA/TiO_2NTAs and Ag/TiO_2NTAs was similar, it does not mean that the particle size of two catalysts was also comparable, since the two photocatalysts were not pulverous, it was not accurate to calculate the size of the whole catalyst. Moreover, the UV–vis characterization might not provide the best resolution into distinguishing slight differences in size/aggregation between two photocatalysts. Based on above analysis, it could be expected that Ag/SCA/TiO_2NTAs should demonstrate a superior photocatalytic activity compared to Ag/TiO_2NTAs.

3.2. *E. coli* inactivation performance

3.2.1. *E. coli* inactivation in the absence of PMS

The *E. coli* inactivation efficiency by the as-prepared photocatalysts under dark (control tests) and VL irradiation was explored, and the results were shown in Fig. 4. As can be seen, VL alone almost does not affect bacteria inactivation within 60 min, indicating that the light intensity and spectral distribution used in this study was not enough to sterilize. This is considered normal, as the lamp type used is a common indoor fluorescent tube. A similar result was also observed in TiO_2NTAs/dark system, manifesting that TiO_2NTAs itself could not inactivate bacteria, and adsorption is negligible. The diameter of the tubes (of the order of 100 nm) does not permit the introduction of the μm cells into the body of the nanotubes, hence no cells are trapped to manifest a high

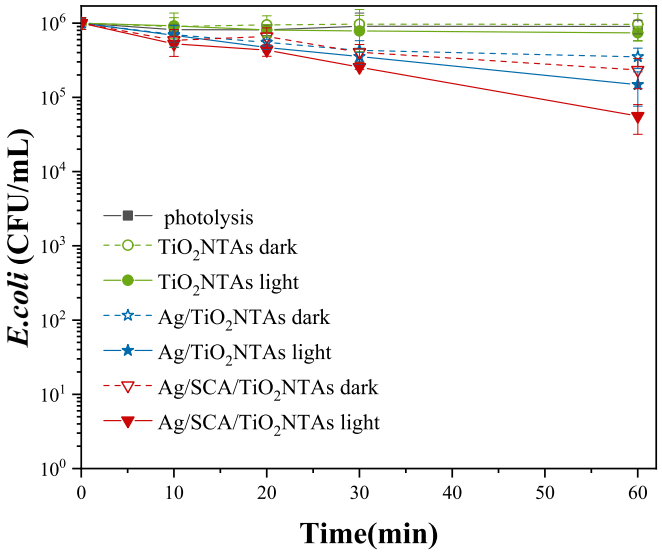

Fig. 4. (Photo) catalytic inactivation of *E. coli* mediated by the as-prepared photocatalysts in dark and visible light irradiation without PMS. Experimental conditions: [bacteria] = 10^6 CFU/mL, [pH] = 7.5. The inactivation experiments were performed in triplicate (the standard error was found to be of ~5 %).

adsorption effect. Additionally, as shown in the SEM image (Fig. S2), TiO_2NTAs were in a regular and ordered tubular arrangement on the Ti substrate, with smooth closed edges, hence the mechanical stress originated from TiO_2NTAs could be considered so minimal that was not enough to inactivate the bacteria.

TiO_2NTAs/VL system exhibited a weak inactivation efficacy, implying that VL at this intensity could not effectively stimulate TiO_2NTAs to produce reactive species. Furthermore, a moderate inactivation effect was observed in both Ag/TiO_2NTAs/dark and Ag/SCA/TiO_2NTAs/dark systems. Since TiO_2NTAs have been shown not to inactivate bacteria, the inactivation performance of the two systems can be ascribed to the antibacterial property of Ag itself and the mechanical stress of the non-SCA-containing photocatalyst (Prabhu and Poulose, 2012). Notably, although the severe Ag agglomerations resulted in less active sites in Ag/TiO_2NTAs, the mechanical stress produced by the sharp edges of metallic Ag aggregates in Ag/TiO_2NTAs (formed by Ag agglomeration, Fig. 2b) could also cause the bacteria to die, leading to similar inactivation results of two systems. The inactivation efficiency of Ag/TiO_2NTAs and Ag/SCA/TiO_2NTAs was further improved under VL irradiation; Ag/TiO_2NTAs/VL and Ag/SCA/TiO_2NTAs/VL systems achieved about 0.9-log and 1.3-log inactivation, respectively, which could be attributed to the photocatalytic activity brought by the SPR effect of AgNPs. Owing to the introduction of SCA, AgNPs were more evenly distributed on TiO_2NTAs, leading to a stronger SPR effect than that of Ag/TiO_2NTAs, and corresponding higher inactivation efficiency. Although the observed inactivation was multiple times higher under VL, this ~90 % elimination (1 log U) is rather low for the needs of water treatment. Hence, its enhancement by oxidant is considered imperative.

3.2.2. *E. coli* inactivation in presence of PMS

Considering the moderate *E. coli* inactivation in oxidant-free systems, PMS introduction in the photo-catalytic process was then investigated. Firstly, the PMS dose was optimized. As shown in Fig. 5a, four concentrations of PMS (0.01 mM, 0.03 mM, 0.05 mM, and 0.1 mM) were used alone or in combination with Ag/SCA/TiO_2NTAs under VL irradiation for *E. coli* inactivation. At PMS concentration of 0.01 mM, there was almost no inactivation in PMS/VL system, implying that PMS at this concentration was not enough to inactivate the existing concentration of bacteria in the system. Ag/SCA/TiO_2NTAs/PMS/VL system exhibits

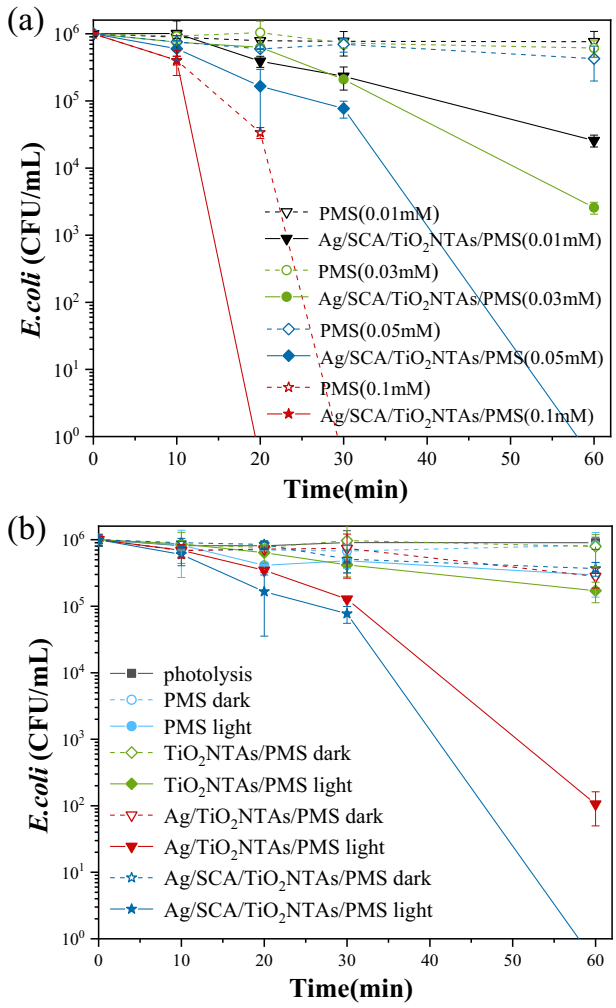

Fig. 5. Effect of PMS concentration on the inactivation performance of the sole PMS system and Ag/SCA/TiO_2NTAs system (a), *E. coli* inactivation in different systems in the presence of PMS (b). Experimental conditions: [bacteria] = 10^6 CFU/mL, [pH] = 7.5, [PMS] = 0.05 mM. The inactivation experiments were performed in triplicate (the standard error was found to be of ~5 %).

about 1.5-log inactivation, which was very close to the result of the Ag/SCA/TiO_2NTAs/VL system, suggesting that at this concentration, Ag/SCA/TiO_2NTAs could not activate PMS effectively for *E. coli* inactivation. When the PMS concentration increased, the inactivation performance in both systems was improved correspondingly. When PMS concentration reached 0.1 mM, the total inactivation of *E. coli* was observed within 30 min in PMS/VL system, effectiveness consistent with literature reports on the efficacy of PMS for disinfection (Berruti et al., 2021). In the case of the Ag/SCA/TiO_2NTAs/PMS/VL system, complete inactivation was observed within 60 min and 20 min at PMS concentrations of 0.05 mM and 0.1 mM, respectively. Additionally, analysis of variance (ANOVA) was conducted to confirm the effect of PMS concentration on *E. coli* inactivation. As shown in Table S2, the *p*-value was <0.05, manifesting the statistically significant difference between PMS concentration and *E. coli* inactivation. The corresponding post hoc tests were shown in Table S3 to disclose the specific concentration groups differed (highlighted in bold). Although Ag/SCA/TiO_2NTAs/PMS/VL system exhibited a faster *E. coli* inactivation at a PMS concentration of 0.1 mM, at this concentration, the pseudo-first-order rate constants (k_{obs}) of Ag/SCA/TiO_2NTAs/PMS/VL system was only 1.6 times higher than that of PMS/VL system (Table 1). This suggests that doubling the concentration did not yield a corresponding effect and the system is no longer efficiently using PMS. However, at a PMS concentration of 0.05

Table 1
Pseudo first-order rate constants (k_{obs}) for *E. coli* inactivation in different systems.

K_{obs} (min^{-1})	System
0.00407 ± 0.0017	PMS/VL (0.01 mM)
0.06457 ± 0.00628	Ag/SCA/TiO_2NTAs/PMS/VL (0.01 mM)
0.00873 ± 0.00261	PMS/VL (0.03 mM)
0.1029 ± 0.01836	Ag/SCA/TiO_2NTAs/PMS/VL (0.03 mM)
0.01266 ± 0.00291	PMS/VL (0.05 mM)
0.24897 ± 0.05124	Ag/SCA/TiO_2NTAs/PMS/VL (0.05 mM)
0.46374 ± 0.17116	PMS/VL (0.1 mM)
0.73169 ± 0.36965	Ag/SCA/TiO_2NTAs/PMS/VL (0.1 mM)

mM, the k_{obs} of Ag/SCA/TiO_2NTAs/PMS/VL system was 19.7 times higher than that of the PMS/VL system. Obviously, the inactivation at a PMS concentration of 0.1 mM was mainly ascribed to the higher PMS dose rather than the synergistic effect between PMS and Ag/SCA/TiO_2NTAs. Therefore, from the system efficiency point of view, a PMS concentration of 0.05 mM was selected as the case-specific optimized concentration and was used in the following tests.

The *E. coli* inactivation in different systems using the optimal PMS dose was then compared and summarized in Fig. 5b. It was observed that the sole PMS in the dark exhibited a poor inactivation ability towards *E. coli*, manifesting that PMS at this concentration was barely able to inactivate *E. coli* via plain oxidation. On the other hand, the PMS/VL system exhibited about 0.5-log inactivation within 60 min. PMS activation driven by VL has been reported by many studies (Liu et al., 2018; Wu et al., 2017; Zhang et al., 2018), the limited inactivation efficiency here might be due to the emitted light spectrum or low concentration of PMS (Ozores Diez et al., 2020). In further control tests, the bacteria could hardly be inactivated in TiO_2NTAs/PMS/dark system, implying that TiO_2NTAs could not activate PMS in the dark, which is consistent with our previous study (Jia et al., 2020b).

Concerning VL-mediated photocatalytic PMS activation, we found that the TiO_2NTAs/PMS/VL system obtained about 0.7-log inactivation. Previous studies have reported that under VL irradiation, TiO_2 could react with PMS to form a complex that shows a higher VL response than PMS alone, then the photoexcited complex would inject the electrons to the conduction bond (CB) of TiO_2NTAs to activate PMS via the ligand-to-metal charge transfer mechanism (Jia et al., 2020b; Jo et al., 2018). Compared to Ag/TiO_2NTAs/dark and Ag/SCA/TiO_2NTAs/dark systems, in the presence of PMS, the inactivation efficiency of both systems showed a negligible improvement, manifesting that neither photocatalyst could activate PMS effectively under dark conditions. As expected, the Ag/TiO_2NTAs/PMS and Ag/SCA/TiO_2NTAs/PMS systems exhibited a dramatic inactivation performance enhancement under VL irradiation, reaching 4-log and 6-log inactivation, respectively, indicating the high PMS activation by Ag/TiO_2NTAs/VL and Ag/SCA/TiO_2NTAs/VL processes. Particularly, Ag/SCA/TiO_2NTAs/PMS/VL system exhibited stronger inactivation effectiveness than that of the Ag/TiO_2NTAs/PMS/VL system, implying that a more efficacy PMS activation was obtained in the Ag/SCA/TiO_2NTAs/PMS/VL system. This could be ascribed to the introduction of SCA; the coupling agent made AgNPs more evenly dispersed on TiO_2NTAs, thus providing more active sites for PMS activation under VL irradiation. Additionally, *t*-test analysis results in different systems revealed the significant difference ($p < 0.05$) (Fig. S7).

The inactivation efficacy of Ag/SCA/TiO_2NTAs in the presence and absence of VL and PMS was also compared and the results were shown in Table 2. Based on previous study, the inactivation efficiency in this work could be calculated by following Eq. (1) (Liu et al., 2021),

$$\text{Inactivation efficiency} = \frac{bacterial\ \ reduction(CFU/mL)}{photocatalyst\ \ concentration(g/L) \times inactivation\ \ time(min)} \quad (1)$$

Table 2
Comparison of the efficacy of Ag/SCA/TiO_2NTA in the presence and absence of VL and PMS (photocatalyst concentration: 0.14 g/L, inactivation time: 60 min).

System	Bacterial reduction (CFU/mL)	Inactivation efficiency (CFU/(g·min))
Ag/SCA/TiO_2NTA	2.51 ± 0.79	$2.99 \times 10^2 \pm 93.55$
Ag/SCA/TiO_2NTA/PMS	3.16 ± 0.63	$3.76 \times 10^2 \pm 74.54$
Ag/SCA/TiO_2NTA/VL	19.9 ± 2.55	$2.38 \times 10^3 \pm 303.52$
Ag/SCA/TiO_2NTA/PMS/VL	$1.00 \times 10^6 \pm 0$	$1.19 \times 10^8 \pm 0$

It can be clearly seen that when in the presence of both VL and PMS, the efficacy of Ag/SCA/TiO_2NTAs has the highest value (1.19×10^8), which was 3.97×10^5, 3.16×10^5 and 5.0×10^4 times higher than that of Ag/SCA/TiO_2NTAs alone, Ag/SCA/TiO_2NTAs/PMS and Ag/SCA/TiO_2NTAs/VL groups, indicating the high synergy of the Ag/SCA/TiO_2NTAs/PMS/VL system. Moreover, a comparison of *E. coli* inactivation by different reported photocatalytic AOPs was conducted and summarized (Table 4). As shown in Table 4, taking the aspects of light intensity, the dose of photocatalyst and PMS, the complexity preparation process of the catalyst, and the reusability of the photocatalyst into consideration comprehensively, it could be confirmed that the Ag/SCA/TiO_2NTAs had a superior performance among most of the listed photocatalysts.

The excellent inactivation performance of the Ag/SCA/TiO_2NTAs/PMS/VL system makes the system a good candidate for environmental applications, if other characteristics also comply, such as its susceptibility to common water constituents, its stability, and reusability. As such, the next tests deal with these aspects.

3.2.3. Reusability and stability experiments

The stability and reusability of catalysts are important features that define their practical applicability in water treatment. Therefore, to explore the potential of the Ag/SCA/TiO_2NTAs/PMS/VL system, cyclic reuse experiments were conducted. For comparison, the Ag/TiO_2NTAs/PMS/VL system was also subjected to perform the cyclic inactivation experiments. As shown in Fig. 6a, after four cycles of use, the Ag/SCA/TiO_2NTAs/PMS/VL system could still attain complete inactivation within 60 min. However, for Ag/TiO_2NTAs photocatalyst, although Ag/TiO_2NTAs/PMS/VL system could completely inactivate bacteria in the first round, its inactivation efficiency was gradually attenuated in the following cycles. After four cycles, the system could only inactivate about 0.8-log *E. coli*, which was almost as same as the TiO_2NTAs/PMS/VL system, hence the catalyst is passivated. For this phenomenon, we suggest that the reduced inactivation performance was attributed to that the Ag NPs falling off from TiO_2NTAs, since there was no binder was used in Ag/TiO_2NTAs photocatalyst.

To confirm this hypothesis and identify the reasons behind the apparent loss of activity, the ICP-MS characterization was conducted to comparatively detect the Ag leaching in the two systems. As displayed in Table 3, the amount of Ag lost in the Ag/TiO_2NTAs/PMS/VL system from the first to the fourth cycle was 8.01, 0.20, 0.05, and 0.004 mg/L, respectively. However, the value identified in Ag/SCA/TiO_2NTAs/PMS/VL system from the first to the fourth cycle was only 0.39, 0.018, 0.004, and 0.001 mg/L, respectively. Additionally, Ag leaching of the two systems in Milli-Q water in the absence of *E. coli* was also conducted, and was shown in Table S1. It can be concluded that the presence or absence of *E. coli* had little effect on Ag leaching, indicating that there is little adsorption or interaction between Ag and *E. coli*. Notably, based on the Table 3, Ag loss percentage of Ag/TiO_2NTAs/PMS/VL system was only

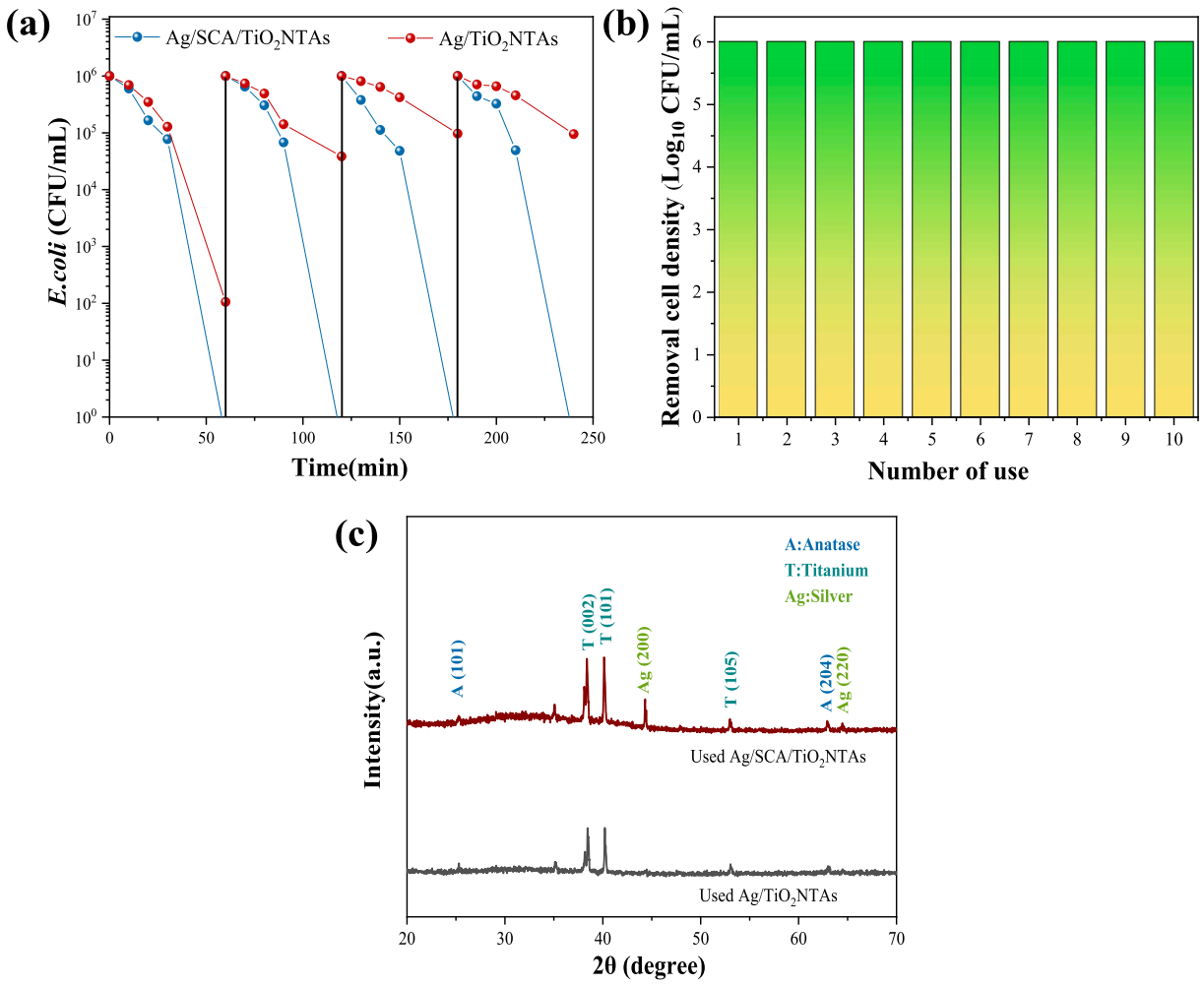

Fig. 6. Cyclic experiments for *E. coli* inactivation in Ag/SCA/TiO_2NTAs/PMS/VL and Ag/ TiO_2NTAs/PMS/VL systems (a), repeated experiments in Ag/SCA/TiO_2NTAs/PMS/VL system for *E. coli* inactivation, each cycle lasted 60 min (b), and XRD patterns of the used Ag/TiO_2NTAs and Ag/SCA/TiO_2NTAs (c). Experimental conditions: [bacteria] = 10^6 CFU/mL, [pH] = 7.5, [PMS] = 0.05 mM. The inactivation experiments were performed in triplicate (the standard error was found to be of ~5 %).

4.6 %, however, the XRD and XPS characterization of the used Ag/TiO_2NTAs indicated that a serious Ag leaching occurred in Ag/TiO_2NTAs. This might be due to that the filtration before the ICP-MS test would trap most of Ag in the Ag/TiO_2NTAs/PMS/VL system, because of the pore size of the filter membrane is 0.22 μm, which is much smaller than the size of most of AgNPs (Figs. 2b and S5a). While, it hardly affects the Ag leaching in Ag/SCA/TiO_2NTAs/PMS/VL system, since the AgNPs sizes of Ag/SCA/TiO_2NTAs were ranged from 13 to 46 nm (Fig. S6), which was much smaller than 0.22 μm. Even so, Ag ion leaching (did not contain leached AgNPs) in the Ag/TiO_2NTAs/PMS/VL system after filtration was much larger than the total Ag leaching in Ag/SCA/TiO_2NTAs/PMS/VL system, which was further clarified the stability of Ag/SCA/TiO_2NTAs photocatalyst. The detected Ag leaching in the system without SCA might also be due to that a part of Ag aggregates dissolve in solution and then pass through the filter membrane. Moreover, the *t*-test results about Ag leaching in the two systems showed the significant difference ($p < 0.05$) (Fig. S8), further demonstrating that SCA could effectively prevent Ag leaching. It was worth noting that the EPA (United. States. Environmental Protection Agency) recommends drinking water contain no >0.05 mg/L of Ag. Therefore, if Ag/SCA/TiO_2NTAs/PMS/VL system was applied in practice, pre-experiment should be conducted several rounds in a specific reactor to avoid the Ag lost exceeding the limit value, and this was also conductive to the subsequent recovery of Ag.

Table 3
Ag leaching in different systems from the first use to fourth use in the presence of *E. coli*.

System	Number of cycles/Ag leaching (mg/L)			
	1	2	3	4
Ag/TiO_2NTAs/PMS/VL	8.01 ± 0.223	0.20 ± 0.015	0.05 ± 0.010	0.004 ± 0.001
Ag/SCA/TiO_2NTAs/PMS/VL	0.39 ± 0.010	0.018 ± 0.001	0.004 ± 0.001	0.001 ± 0.0001

Ag/TiO_2NTAs/PMS/VL system:
Ag loss content in = (8.01 + 0.2 + 0.05 + 0.004) mg/L * (1 L/1000 mL) * 50 mL = 0.41 mg.
Ag loss ratio = 0.41/9 × 100 % = 4.6 %.
Ag/SCA/TiO_2NTAs/PMS/VL system:
Ag loss content in = (0.41 + 0.021 + 0.004 + 0.001) mg/L * (1 L/1000 mL) * 50 mL = 0.02 mg.
Ag loss ratio = 0.02/5 × 100 % = 0.4 %.

The ICP-MS results verified our speculation and demonstrated the high reusability of Ag/SCA/TiO_2NTAs. The high reusability of Ag/SCA/TiO_2NTAs could be ascribed to the 'bridging' effect brought by SCA (Sang et al., 2017; Zheng et al., 2019), in which the silanol hydroxyl groups of SCA could connect with TiO_2NTAs, and the vinyl group of SCA could coordinate the AgNPs (Burgess and Steel, 2011; Fu et al., 2021), in

Table 4
Comparation of different photocatalytic AOPs towards *E. coli* inactivation under visible light irradiation.

Photocatalyst	Light intensity (W/m^2)	Photocatalyst concentration (g/L)	PMS (mg/L)	Inactivation time (min)	Bacterial reduction (CFU/mL)	Inactivation efficiency (CFU/(g·min))	Cycle index	Ref
Chlorella @Fe_3O_4@BiOCl	1000	1.0	–	60	10^6	1.67×10^7	4	Xu et al., 2022
La-doped CeO_2	46.5 ± 0.6	4.0	–	150	10^4	1.67×10^4	6	Chatterjee et al., 2023
P/Ag/Ag_2O/Ag_3PO_4/TiO_2	750	0.5	–	20	10^7	1.00×10^9	5	Liu et al
Ag/g-C_3N_4	2710	0.1	–	120	10^7	8.33×10^8	4	Wei et al., 2020
CeO_2/g-C_3N_4	1760	0.2	–	180	10^7	2.78×10^8	Unknown	Huang et al., 2021
GO/TiO_2	500	1.05	–	30	10^3	3.17×10^4	Unknown	Ch-Th et al., 2021
3D-rGO	380	0.001	10	30	2×10^6	6.67×10^{10}	Unknown	Karbasi et al., 2020
N-MgO@Fe_3O_4	430	0.1	75	15	10^6	6.67×10^8	Unknown	Akbari et al., 2022
Cu-TCPP(BA)-MOF	2000	0.094	94.3	50	10^7	4.70×10^{10}	5	Bai et al., 2022
g-C_3N_4	1500	0.1	153.5	120	10^5	8.33×10^6	5	Zhang et al., 2021
Ag/SCA/TiO_2NTAs	93.5 ± 0.5	0.14	15.35	60	10^6	1.19×10^8	10	This work

this way, the adhesion strength between Ag and TiO_2NTAs was greatly improved, resulting in a highly reusable catalyst. It was worth noting that the maximum leaching of Ag^+ in the Ag/SCA/TiO_2NTAs/PMS/VL system was 0.39 mg/L, which was lower than the suggested Minimum Inhibitory Concentration of Ag^+ for *E. coli* (0.78 mg/L) (Liu et al., 2021), implying that the effective inactivation of Ag/SCA/TiO_2NTAs/PMS/VL system was mainly ascribed to photocatalytic oxidation performance of the system, rather than any homogeneous the antibacterial effect brought by the released Ag^+ from the catalyst. In addition, it was found that the Ag/SCA/TiO_2NTAs/PMS/VL system could still achieve 6-log inactivation after ten cycles of uses (Fig. 6b), manifesting the excellent reusability Ag/SCA/TiO_2NTAs possesses.

Furthermore, to explore the physicochemical stability of photocatalyst, a series of characterization of Ag/SCA/TiO_2NTAs before and after the reaction were provided. As can be seen, the XRD patterns (Fig. 6c) were almost identical before and after four cycles of use. In addition, although the XPS survey demonstrated that the chemical composition of the sample was the same before and after used (Fig. S3a), the peak intensity of Ag 3d after used was a little weaker than the fresh one. Likewise, the UV–vis DRS spectrum showed that in the VL region, the peak intensity of the used Ag/SCA/TiO_2NTAs was a slight decrease compared to the fresh one (Fig. S3b). The above phenomena could also be ascribed to the loss of Ag. Even so, the used Ag/SCA/TiO_2NTAs was still displayed a relatively intense absorption in the VL region, suggesting the good stability of the catalyst. The above description indicates that Ag/SCA/TiO_2NTAs possesses highly stable physicochemical properties. Combining the facile preparation, no need for separation (as slurry TiO_2 needs), and high recycling ability, the developed photocatalytic system may serve as a good candidate in a real environment for efficiency and sustainable application.

3.3. Pathways and species involved in E. coli inactivation

To identify the possible reactive species involved in Ag/SCA/TiO_2NTAs/PMS/VL system, different quenchers were employed to trap potential reactive species. It should be noted that in these scavenging experiments, the chosen quenchers should have no toxicity towards bacteria. Therefore, based on previous studies, NaCl, isopropanol, sodium oxalate, superoxide dismutase (SOD), and L-histidine were chosen as quenchers for $SO_4^{\bullet-}$, •OH, h^+, $O_2^{\bullet-}$ and $^1O_2$, respectively, and the concentration limits of each the quencher were also verified to be harmless to bacteria in control tests (Jiang et al., 2022; Karbasi et al., 2020; Kohantorabi et al., 2021a). As shown in Fig. 7a, there was significant scavenging of the inactivation effect, but no big difference in inactivation efficiency between the tests where NaCl and isopropanol were added into the system; the inactivation rate was reduced by about 3.3-log and 3.5-log, respectively, suggesting that both $SO_4^{\bullet-}$ and •OH contributed to *E. coli* inactivation during the reaction process. Sodium oxalate exhibited a lower inhibition on inactivation rate (about 2-log), implying that h^+ was also involved in *E. coli* inactivation, but made less contribution compared to $SO_4^{\bullet-}$ and •OH. When SOD was introduced into the system, the bacteria could still be completely inactivated within 60 min, thus ruling out the participation of $O_2^{\bullet-}$, but raises the question of singlet oxygen participation. For this species, after L-Histidine was introduced into the system, the inactivation rate was reduced by about 4-log, indicating that $^1O_2$ might be involved in *E. coli* inactivation since L-Histidine could also react with PMS and therefore decrease the inactivation rate. To further confirm the role of $^1O_2$, the inactivation experiment was also performed in D_2O, since the lifetime of $^1O_2$ in D_2O is 10 times longer than that of H_2O (Yun et al., 2018). As displayed in Fig. 7b, *E. coli* inactivation in D_2O was faster than that of H_2O, demonstrating that $^1O_2$ was indeed involved in the inactivation. Based on the above results, it can be preliminarily inferred that $SO_4^{\bullet-}$, •OH, h^+, and $^1O_2$ were all involved in *E. coli* inactivation in the Ag/SCA/TiO_2NTAs/PMS/VL system.

The EPR measurements were conducted to further explore the reactive species by using DMPO and TEMP as spin trapping reagents. It can be clearly seen from Fig. 7c that none of the characteristic peaks of reactive species appeared in the DMPO group in the dark. With the light was turned on, a distinctive signal with quadruple peaks, and with an intensity ratio of 1:2:2:1 appeared, which is ascribed to the characteristic peaks of DMPO-•OH and DMPO-$SO_4^{\bullet-}$ adducts (Wang et al., 2014). There were no characteristic signals of $O_2^{\bullet-}$ emerging in the system (data not shown), which was consisted with the result of the quenching experiments. In addition, a triple peak signal with a ratio of 1:1:1 was observed in Fig. 7d, which could be assigned to the characteristic peaks of TMP-$^1O_2$ (Zhou et al., 2015).

Table 5
Physicochemical characteristics of the waters used in the experiments.

Parameter	Milli-Q water	Tap water
pH	6.5	7.3
TOC (mg/L)	<0.05	1.7–2.4
Chloride (Cl^-, mg/L)	–	11–24
Sulfate (SO_4^{2-}, mg/L)	–	3.0–19
Nitrate (NO_3^-, mg/L)	–	1.0–7

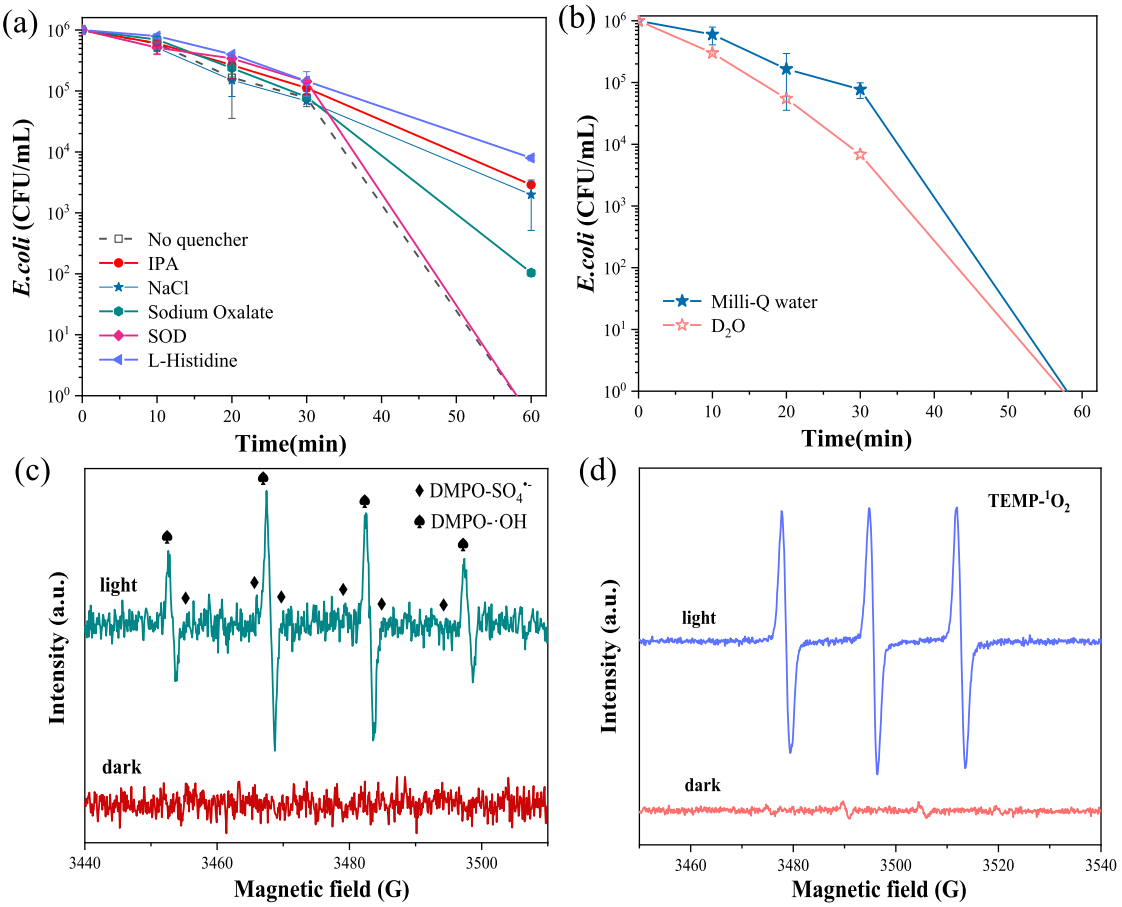

Fig. 7. Effects of various quenchers on *E. coli* inactivation (a); *E. coli* inactivation in H_2O and D_2O (50 %) systems (b); DMPO (c) and TEMP (d) spin-trapping EPR spectra. Experimental conditions: Ag/SCA/TiO_2NTAs/PMS system, [bacteria] = 10^6 CFU/mL, $[PMS]_0$ = 0.05 mM, [NaCl] = 0.3 mM, [IPA] = 0.3 mM, [Sodium Oxalate] = 0.3 mM, [SOD] = 50 units/mL, [L-Histidine] = 10 mM, T = 25 °C. Experimental conditions: [bacteria] = 10^6 CFU/mL, [pH] = 7.5, [PMS] = 0.05 mM. The inactivation experiments were performed in triplicate (the standard error was found to be of ~5 %).

Among the four tested reactive species, the source of $^1O_2$ is worthy of further investigation, since the source and generation of the other three reactive species can be easily inferred. In general, as a precursor of $^1O_2$, $O_2^{\bullet-}$ can induce the production of $^1O_2$ (Dong et al., 2020; Zhou et al., 2022). However, the quenching tests and EPR measurements have revealed that $O_2^{\bullet-}$ was not present in the system. Therefore, there must be another way that exists in the system to induce the formation of $^1O_2$. Gao et al. (2019) used perovskite to activate PMS to degrade ofloxacin and found that $^1O_2$ could be generated by PMS and oxygen vacancies (Ov) of perovskite, and the amount of $^1O_2$ is positively correlated with the concentration of Ov. Inspired by this, it was reasonable to deduce that Ov could also be formed in Ag/SCA/TiO_2NTAs during the reaction process, which was then reacted with PMS to induce the formation of $^1O_2$. Thus, to prove this speculation, the high-resolution XPS spectra of O1s and Ag3d in the used Ag/SCA/TiO_2NTAs were also analyzed and compared with the fresh one. As depicted in Fig. 3d, in O1s high-resolution spectrum, no characteristic peaks of Ov (531.0 eV) were observed in the fresh sample, while it was found in the used one, manifesting that Ov was formed during the reaction. Additionally, in the Ag3d high-resolution XPS spectra (Fig. 3b), the characteristic peaks of Ag^+ appeared in the used Ag/SCA/TiO_2NTAs (peaks at 367.5 eV and 373.5 eV) (Thomas et al., 2012). However, no characteristic peak of Ov was observed in the used Ag/TiO_2NTAs (Fig. S4), and the characteristic peak of Ag disappeared, which could be due to the serious Ag leaching without SCA (Jia et al., 2023). Moreover, no Ag—O bond (528.5 eV) was found in the O1s high-resolution XPS spectra of the used Ag/SCA/TiO_2NTAs (Fig. 3d), this precluded the presence of Ag_2O (Cui et al., 2017), indicating that the Ag^+ generated in the catalyst was not converted into Ag oxide, which indirectly proved the possibility formation of Ov.

In the same line of work, Li et al. (2020) found that during the synthetic process of Ag-doped ZnO by an electrochemical deposition method, when Ag^+ replaced Zn^{2+} in ZnO, Ov could be formed owing to the difference of valence state between Ag^+ and Zn^{2+}. Likewise, in this work, during the photo-deposition process, Ag^+ could also replace Ti^{4+}, resulting in the formation of Ov due to the difference in the valence state between Ag^+ and Ti^{4+}. Thus, the discovery of Ag^+ in the used Ag/SCA/TiO_2NTAs could be further evidence for the existence of Ov. Based on the XPS analysis, it can be concluded that Ov was formed in Ag/SCA/TiO_2NTAs during the reaction process, which was then leading to the generation of $^1O_2$ by reacting with PMS.

Based on the above analysis, the probable inactivation mechanism of Ag/SCA/TiO_2NTAs/PMS/VL system was proposed. As depicted in Fig. 8, by using SCA as a binder, AgNPs were firmly fixed on TiO_2NTAs surface. In addition to the inactivation effect brought by Ag itself (a very minor part as discussed in 3.3.1), the bacteria inactivation was mainly attributed to the reactive species generated in the system. Owing to the introduction of SCA, AgNPs could be well dispersed on the surface of TiO_2NTAs in the form of Ag^0, and thanks to the SPR effect brought by AgNPs, the photo-excited electrons (e^-) could be injected into the CB of TiO_2NTAs directly. In this way, the photo-excited electron-hole pairs could be effectively separated (Eq. (2)). Then, the holes (h^+) accumulated on TiO_2NTAs could inactivate *E. coli* directly on the surface of Ag/SCA/TiO_2NTAs, or react with the adsorbed H_2O or -OH to generate •OH

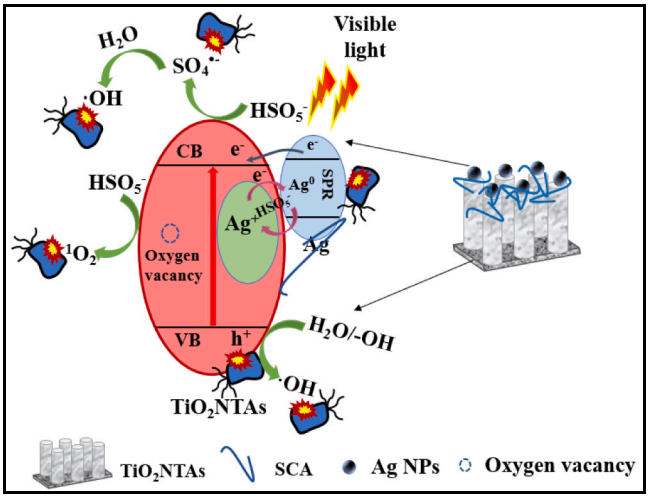

Fig. 8. Proposed mechanism of *E. coli* inactivation in Ag/SCA/TiO_2NTAs/PMS/VL system.

(Eq. (3)). As an electron acceptor, PMS could trap e^- to produce $SO_4^{\bullet-}$ (Eq. (4)), which further promote the separation of photo-generated carriers, and $SO_4^{\bullet-}$ could also react with H_2O to form •OH (Eq. (5)). Besides, Ag^0 could activate PMS to generate $SO_4^{\bullet-}$, during this process, Ag^0 transformed to Ag^+ (Eq. (6)), Ag^+ could replace Ti^{4+} sites in TiO_2 and leading to the formation of Ov. Then, $^1O_2$ would be generated by the reaction between Ov and PMS (Eq. (7)) (Gao et al., 2019). Meanwhile, a part of Ag^+ would be reduced by e^-/PMS to Ag^0 again (Eqs. (8) and (9)) (Jia et al., 2023). Owing to the introduction of SCA, the regenerated Ag^0 would be firmly fixed on the surface of TiO_2NTAs, and scarcely leaching into the solution, then repeated the reaction of Eq. (6) to Eq. (9), forming a stable $Ag^0 \leftrightarrow Ag^+$ cycle in the Ag/SCA/TiO_2NTAs/PMS/VL system (Jia et al., 2023), hence the homogeneous reactions are negligible, and it is the catalyst leading the highly effective inactivation of *E. coli*.

$$Ag/SCA/TiO_2NTAs + h\nu \rightarrow e^- + h^+ \quad (2)$$

$$h^+ + H_2O/-OH \rightarrow \dot{O}H + H^+ \quad (3)$$

$$HSO_5^- + e^- \rightarrow SO_4^{\bullet-} + OH^- \quad (4)$$

$$SO_4^{\bullet-} + H_2O \rightarrow H^+ + SO_4^{2-} + \dot{O}H \quad (5)$$

$$Ag^0 + HSO_5^- \rightarrow Ag^+ + SO_4^{\bullet-} + OH^- \quad (6)$$

$$O_V + HSO_5^- \rightarrow {}^1O_2 + HSO_4^- \quad (7)$$

$$Ag^+ + HSO_5^- \rightarrow Ag^0 + SO_5^{\bullet-} + H^+ \quad (8)$$

$$Ag^+ + e^- \rightarrow Ag^0 \quad (9)$$

3.4. Effect of water matrices on E. coli inactivation

To evaluate the possibility to apply this catalyst in real water matrices, the effects of naturally encountered inorganic anions on *E. coli* inactivation in Ag/SCA/TiO_2NTAs/PMS/VL system were explored,

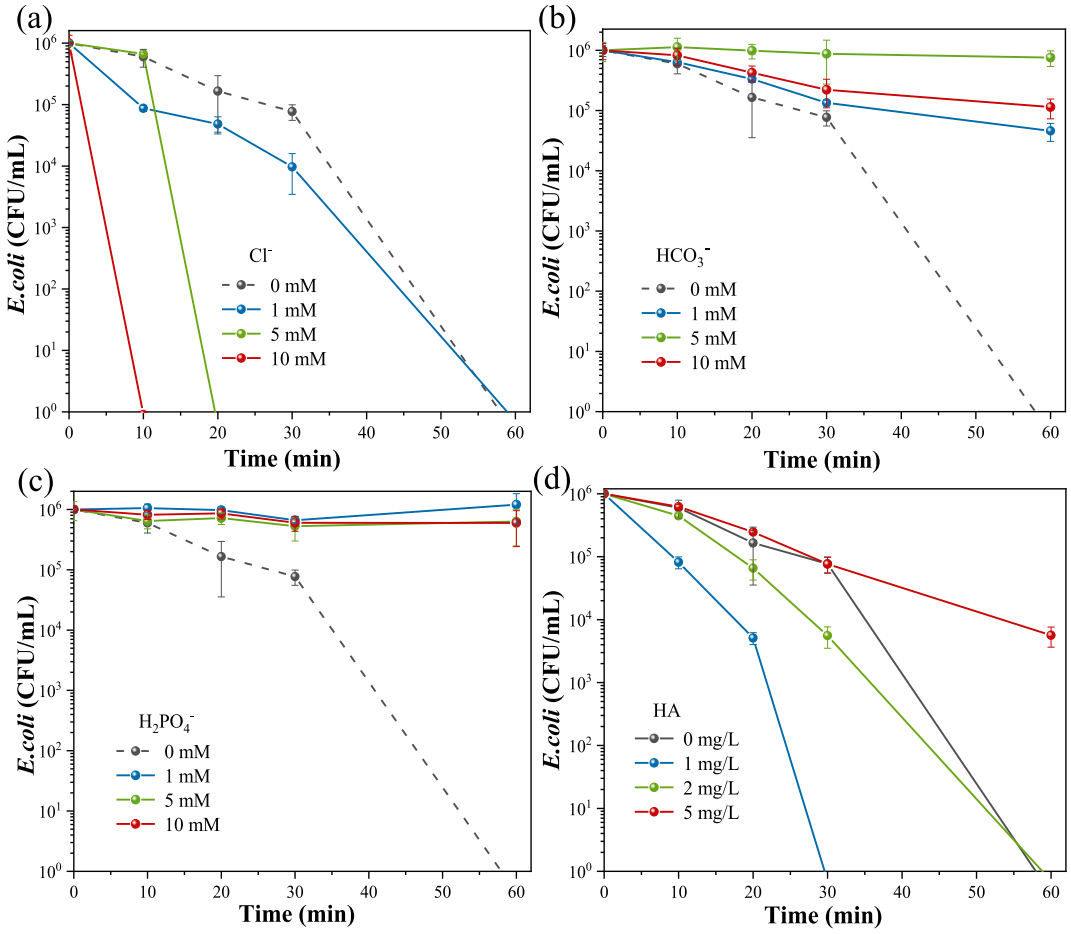

Fig. 9. Effects of (a) Cl^-, (b) HCO_3^-, (c) $H_2PO_4^-$ and (d) HA on the inactivation efficiency of Ag/SCA/TiO_2NTAs/PMS/VL system, Experimental conditions: [bacteria] = 10^6 CFU/mL, [pH] = 7.5, [PMS] = 0.05 mM. The inactivation experiments were performed in triplicate (the standard error was found to be of ~5 %).

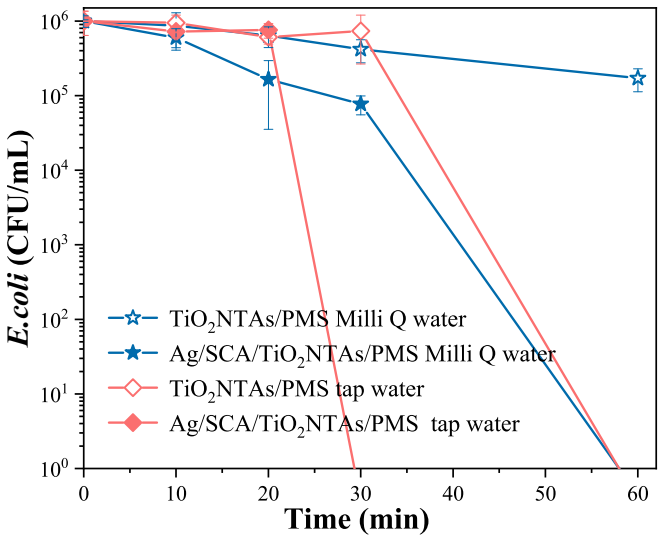

Fig. 10. The inactivation efficiency of TiO_2NTAs/PMS/VL and Ag/SCA/TiO_2NTAs/PMS/VL systems in different water bodies. Experimental conditions: [bacteria] = 10^6 CFU/mL, [pH] = 7.5, [PMS] = 0.05 mM. The inactivation experiments were performed in triplicate (the standard error was found to be of ~5 %).

three common inorganic salts, i.e., NaCl, $NaHCO_3$ and NaH_2PO_4 were spiked into the reaction system. In addition, since the organic contaminants are usually present along with microbial agents in aqueous matrices, humic acid (HA), one of the most common NOM in natural water bodies was chosen as a representative organic compound to evaluate the effect of organic contaminants on the inactivation efficiency of *E. coli* in the developed system. The inactivation efficiency of *E. coli* with different amounts of inorganic ions and HA were studied and the results were displayed in Fig. 9.

As displayed in Fig. 9a, with the Cl^- concentration increased from 0 to 10 mM, the inactivation efficiency was significantly improved. At the concentration of 10 mM, the bacteria could be totally inactivated within 10 min. This could be ascribed to the fact that the concentration of Cl^- (1 mM, 5 mM, and 10 mM) was much higher compared to the concentration of PMS (0.05 mM) used in the system. The excess Cl^- could induce the formation of Cl^- based radicals, HOCl and Cl_2, which can participate in *E. coli* inactivation (Anipsitakis et al., 2008; Liang et al., 2006). Notably, in the quenching experiments, the addition of NaCl inhibited the *E. coli* inactivation; this could be ascribed to the concentration of NaCl used in the quenching experiments, which was only 0.3 mM. At low concentrations, Cl^- could react with $SO_4^{\bullet-}$ to generate chlorine radicals, but not in excess. Compared with $SO_4^{\bullet-}$, these chlorine radicals own a lower oxidation potential, thereby restraining *E. coli* inactivation (Anipsitakis et al., 2008).

HCO_3^- showed an inhibitory effect on the inactivation of *E. coli* (Fig. 9b). With the concentration increase from 0 to 5 mM, the inactivation of *E. coli* was almost completely inhibited. This phenomenon could be attributed to: (i) the role of (bi) carbonate as a quencher for $SO_4^{\bullet-}$ and •OH; HCO_3^- could react with the two radicals to generate $CO_3^{\bullet-}$, which, despite its long lifetime, it possesses a lower oxidation ability compared with •OH and $SO_4^{\bullet-}$ (Hu and Long, 2016), thus suppressed the inactivation; (ii) HCO_3^- might have complexed with Ag metal (Huang et al., 2016); this would destroy the $Ag^0 \leftrightarrow Ag^+$ cycle in the system as discussed in Section 3.3, resulting in the less production of reactive species in the system. It should be noted that with the concentration of HCO_3^- further improved to 10 mM, a small number of bacteria were inactivated, this might be due to that the high concentration of HCO_3^- increased the pH of the system (about 10.7). This pH condition is outside the normal survival margin for *E. coli* (pH:4–9), and may cause inactivation due to protein denaturation.

As depicted in Fig. 9c, three different concentrations of $H_2PO_4^-$ all exhibited complete inhibition of *E. coli* inactivation. This could be explained by the fact that $H_2PO_4^-$ is also a quencher for $SO_4^{\bullet-}$ and •OH (Oh et al., 2016). In addition, $H_2PO_4^-$ might also react with Ag metal to form a complex by chelating reaction (Qi et al., 2014), the generated complex would occupy the active reaction sites on the surface of Ag/SCA/TiO_2NTAs, this would terminate the generation of reactive species in the system, thus retarding *E. coli* inactivation.

Fig. 9d depicts the effects of HA of different concentrations on *E. coli* inactivation in Ag/SCA/TiO_2NTAs/PMS/VL system. As it can be seen, when 1 mg/L of HA was introduced to the system, the inactivation efficiency of *E. coli* was greatly improved, with 6-log inactivation was achieved within 30 min. This was attributed to that HA could be excited under VL irradiation, then PMS could be activated by the VL-excited HA to generate a series of reactive species for the oxidation of the targets in the system (Jia et al., 2020a). However, with the concentration of HA increased from 2 to 5 mg/L, the inactivation efficiency showed a decreasing tendency. The reason could be ascribed to the excess HA: (i) it can occupy the reactive sites of the photocatalyst to reduce the formation of reactive species, (ii) it could cause a light shielding effect, which would reduce the light absorption of the system, resulting in less photons available for the photocatalytic reactions in the system. Besides, one-way ANOVA results show that all *p*-values of above factors were $<$ 0.05 (Table S2), indicating the statistically significant differences between the concentration of the above water matrix (inorganic anions and HA) and *E. coli* inactivation. The corresponding post hoc tests were also conducted to show the specific concentration groups differed (highlighted in bold, Table S4-S7).

To further evaluate the practical application of the constructed system, it is necessary to investigate the disinfection performance of the system in actual water bodies. As discussed above, the system may not work in high levels of inorganic salt since two of the three inorganic salts inhibited the inactivation performance of the system, therefore, the tap water of Madrid was employed and was compared with Milli-Q water. As shown in Fig. 10, when in tap water, the inactivation performance of both TiO_2NTAs/PMS/VL system and Ag/SCA/TiO_2NTAs/PMS/VL system was significantly enhanced, with the complete inactivation achieved within 30 min and 60 min, respectively, which was faster than that of Milli Q water system. Based on the properties of tap water (Table 5) and the analysis above, in addition to the facilitating effect brought by Cl^-, a small amount of the dissolved organic matter in tap water might be also responsible for the enhanced inactivation efficiency as discussed in the HA effect section. The above results manifested that Ag/SCA/TiO_2NTAs/PMS/VL system may act as a good candidate for tap water or even upstream treatment during the drinking water treatment train.

4. Conclusions

In conclusion, the use of SCA as a binder to immobilize AgNPs on TiO_2NTAs led to excellent performance and stability of the photocatalyst to effectively photo-catalyze bacterial disinfection, and the inactivation efficiency was greatly enhanced after PMS was added to the system. Ag/SCA/TiO_2NTA/PMS/VL system possesses excellent stability and reusability, after 10 consecutive runs, 6-logU bacterial inactivation could still be achieved with minimal Ag leaching. The mechanism study suggested that both radical ($SO_4^{\bullet-}$, •OH) and non-radical (h^+, $^1O_2$) pathways were attributed to inducing *E. coli* inactivation. The effect of inorganic anions experiments demonstrated that Cl^- considerably promote the inactivation of the system, while HCO_3^- and $H_2PO_4^-$ exhibited inhibitory effect. The low dose of HA facilitated the inactivation processes, while the higher dose suppressed the bacteria inactivation. Taking into account the facile preparation processes, high inactivation efficiency, excellent stability, and good performance in actual water matrix, the present newly developed SCA immobilized Ag/TiO_2NTAs photocatalyst can be expected to be a bright candidate for sustainable environmental practical application.

CRediT authorship contribution statement

Jialin Jia: Investigation, Methodology, Formal analysis, Writing – original draft. **Stefanos Giannakis:** Conceptualization, Validation, Writing – review & editing. **Dong Li:** Methodology, Writing – review & editing. **Boyin Yan:** Methodology, Formal analysis. **Tao Lin:** Writing – review & editing, Funding acquisition.

Declaration of competing interest

The authors declare that they have no known competing financial interests or personal relationships that could have appeared to influence the work reported in this paper.

Data availability

No data was used for the research described in the article.

Acknowledgments

This work was supported by the funds of the National Key P&D Program of China (2022YFC3203702), the Science and Technology Development Plans of Ministry of Housing and Urban-Rural Development (2021-K-131), the Six Talent Peaks Project in Jiangsu Province (JNHB-004), China Scholarship Council (No. 202006120369), and open research fund project of Key Laboratory of Integrated Regulation and Resources Development of Shallow Lakes of Ministry of Education, Hohai University. Stefanos Giannakis acknowledges the Spanish Ministry of Science, Innovation and Universities (MICIU) for the Ramón y Cajal Fellowship (RYC2018-024033-I). We also acknowledge the Scientific Compass Testing Organization for the ICP-MS measurement.

Appendix A. Supplementary data

Supplementary data to this article can be found online at https://doi.org/10.1016/j.scitotenv.2023.166376.

References

Ahmed, G., Hanif, M., Zhao, L., Hussain, M., Khan, J., Liu, Z., 2016. Defect engineering of ZnO nanoparticles by graphene oxide leading to enhanced visible light photocatalysis. J. Mol. Catal. A Chem. 425, 310–321.

Akbari, S., Moussavi, G., Decker, J., Marin, M.J., Bosca, F., Giannakis, S., 2022. Superior visible light-mediated catalytic activity of a novel N-doped, Fe3O4-incorporating MgO nanosheet in presence of PMS: Imidacloprid degradation and implications on simultaneous bacterial inactivation. Appl. Catal. B Environ. 317, 121732.

Andersson, M., Österlund, L., Ljungström, S., Palmqvist, A., 2002. Preparation of nanosize anatase and rutile TiO2 by hydrothermal treatment of microemulsions and their activity for photocatalytic wet oxidation of phenol. J. Phys. Chem. B 106, 10674–10679.

Anipsitakis, G.P., Dionysiou, D.D., 2003. Degradation of organic contaminants in water with sulfate radicals generated by the conjunction of peroxymonosulfate with cobalt. Environ. Sci. Technol. 37, 4790–4797.

Anipsitakis, G.P., Tufano, T.P., Dionysiou, D.D., 2008. Chemical and microbial decontamination of pool water using activated potassium peroxymonosulfate. Water Res. 42, 2899–2910.

Bai, Y., Nie, G.Z., He, Y., Li, C., Wang, X.B., Ye, L.Q., 2022. Cu-MOF for effectively organic pollutants degradation and E. coli inactivation via catalytic activation of peroxymonosulfate. J. Taiwan Inst. Chem. Eng. 132, 104154.

Bel Hadjltaief, H., Ben Zina, M., Galvez, M.E., Da Costa, P., 2016. Photocatalytic degradation of methyl green dye in aqueous solution over natural clay-supported ZnO–TiO2 catalysts. J. Photochem. Photobiol. A Chem. 315, 25–33.

Berruti, I., Oller, I., Polo-López, M.I., 2021. Direct oxidation of peroxymonosulfate under natural solar radiation: accelerating the simultaneous removal of organic contaminants and pathogens from water. Chemosphere 279, 130555.

Burgess, J., Steel, P.J., 2011. Is the silver–alkene interaction a useful new supramolecular synthon? Coord. Chem. Rev. 255, 2094–2103.

Chatterjee, M., Mondal, M., Sukul, T., Mal, S., Ghosh, K., Das, S., Pradhan, S.K., 2023. Superior photocatalytic performance and photo disinfection of bacteria of solvothermally synthesized mesoporous La-doped CeO2 under simulated visible light irradiation for wastewater treatment. J. Alloys Compd. 942, 169135.

Chen, J., Che, H., Huang, K., Liu, C., Shi, W., 2016. Fabrication of a ternary plasmonic photocatalyst CQDs/Ag/Ag2O to harness charge flow for photocatalytic elimination of pollutants. Appl. Catal. B Environ. 192, 134–144.

Chen, H., Lin, T., Wang, P.F., Zhang, X., Jiang, F.C., Liu, W., 2022. Treatment of bromate in UV/sulfite autoxidation process enhances formation of dibromoacetonitrile during chlorination. Water Res. 225, 119207.

Chen, H., Lin, T., Wang, P.F., Zhang, X., Jiang, F.C., Wang, Y.C., 2023. Novel solar/sulfite advanced oxidation process for carbamazepine degradation: radical chemistry, transformation pathways, influence on disinfection byproducts and toxic changes. Chem. Eng. J. 451, 138634.

Ch-Th, T., Manisekaran, R., Santoyo-Salazar, J., Schoefs, B., Velumani, S., Castaneda, H., Jantrania, A., 2021. Graphene oxide decorated TiO2 and BiVO4 nanocatalysts for enhanced visible-light-driven photocatalytic bacterial inactivation. J. Photochem. Photobiol. A: Chem. 418, 113374.

Cui, Y., Ma, Q., Deng, X., Meng, Q., Cheng, X., Xie, M., et al., 2017. Fabrication of ag-Ag2O/reduced TiO2 nanophotocatalyst and its enhanced visible light driven photocatalytic performance for degradation of diclofenac solution. Appl. Catal. B Environ. 206, 136–145.

Delnavaz, M., Ayati, B., Ganjidoust, H., Sanjabi, S., 2015. Application of concrete surfaces as novel substrate for immobilization of TiO2 nano powder in photocatalytic treatment of phenolic water. J. Environ. Health Sci. Eng. 13, 58.

Dong, X., Duan, X., Sun, Z., Zhang, X., Li, C., Yang, S., et al., 2020. Natural illite-based ultrafine cobalt oxide with abundant oxygen-vacancies for highly efficient Fenton-like catalysis. Appl. Catal. B Environ. 261, 118214.

Fu, S., Zhao, X., Zhou, Z., Li, M., Zhu, L., 2021. Effective removal of odor substances using intimately coupled photocatalysis and biodegradation system prepared with the silane coupling agent (SCA)-enhanced TiO2 coating method. Water Res. 188, 116569.

Gao, P., Tian, X., Nie, Y., Yang, C., Zhou, Z., Wang, Y., 2019. Promoted peroxymonosulfate activation into singlet oxygen over perovskite for ofloxacin degradation by controlling the oxygen defect concentration. Chem. Eng. J. 359, 828–839.

Giannakis, S., Lin, K.-Y.A., Ghanbari, F., 2021. A review of the recent advances on the treatment of industrial wastewaters by sulfate radical-based advanced oxidation processes (SR-AOPs). Chem. Eng. J. 406, 127083.

Giannakis, S., Gupta, A., Pulgarin, C., Imlay, J., 2022. Identifying the mediators of intracellular E. coli inactivation under UVA light: the (photo) Fenton process and singlet oxygen. Water Res. 221, 118740.

Hajjaji, A., Elabidi, M., Trabelsi, K., Assadi, A.A., Bessais, B., Rtimi, S., 2018. Bacterial adhesion and inactivation on ag decorated TiO2-nanotubes under visible light: effect of the nanotubes geometry on the photocatalytic activity. Colloids Surf. B: Biointerfaces 170, 92–98.

Ho, C.-C., Kang, F., Chang, G.-M., You, S.-J., Wang, Y.-F., 2019. Application of recycled lanthanum-doped TiO2 immobilized on commercial air filter for visible-light photocatalytic degradation of acetone and NO. Appl. Surf. Sci. 465, 31–40.

Hu, P., Long, M., 2016. Cobalt-catalyzed sulfate radical-based advanced oxidation: a review on heterogeneous catalysts and applications. Appl. Catal. B Environ. 181, 103–117.

Huang, Z., Yao, Y., Lu, J., Chen, C., Lu, W., Huang, S., et al., 2016. The consortium of heterogeneous cobalt phthalocyanine catalyst and bicarbonate ion as a novel platform for contaminants elimination based on peroxymonosulfate activation. J. Hazard. Mater. 301, 214–221.

Huang, W.Q., Ruan, S.H., Zhao, M.J., Xu, R.S., Chen, Z.Q., G ZH, Song HY., 2021. Visible-light-driven photocatalytic inactivation of *Escherichia coli* by 0D/2D CeO2/g-C3N4 heterojunction: bactericidal performance and mechanism. Journal of environmental. Chem. Eng. 9, 106759.

Ji, H., Lyu, L., Zhang, L., An, X., Hu, C., 2016. Oxygen vacancy enhanced photostability and activity of plasmon-ag composites in the visible to near-infrared region for water purification. Appl. Catal. B Environ. 199, 230–240.

Jia, J., Liu, D., Tian, J., Wang, W., Ni, J., Wang, X., 2020a. Visible-light-excited humic acid for peroxymonosulfate activation to degrade bisphenol a. Chem. Eng. J. 400, 125853.

Jia, J., Liu, D., Wang, S., Li, H., Ni, J., Li, X., et al., 2020b. Visible-light-induced activation of peroxymonosulfate by TiO_2 nano-tubes arrays for enhanced degradation of bisphenol A. Sep. Purif. Technol. 253, 117510.

Jia, J., Giannakis, S., Li, D., Lin, T., Tian, J., Liu, D., et al., 2023. KH570 firmly anchors ag +/Ag0 on TiO2 nanotubes to enhance organics removal during photocatalytic activation of peroxymonosulfate. Sep. Purif. Technol. 124029.

Jiang, Y., Xiong, Z., Huang, J., Yan, F., Yao, G., Lai, B., 2022. Effective E. coli inactivation of core-shell ZnO@ZIF-8 photocatalysis under visible light synergize with peroxymonosulfate: efficiency and mechanism. Chin. Chem. Lett. 33, 415–423.

Jo, Y., Kim, C., Moon, G.-H., Lee, J., An, T., Choi, W., 2018. Activation of peroxymonosulfate on visible light irradiated TiO2 via a charge transfer complex path. Chem. Eng. J. 346, 249–257.

Karbasi, M., Karimzadeh, F., Raeissi, K., Giannakis, S., Pulgarin, C., 2020. Improving visible light photocatalytic inactivation of E. coli by inducing highly efficient radical pathways through peroxymonosulfate activation using 3-D, surface-enhanced, reduced graphene oxide (rGO) aerogels. Chem. Eng. J. 396, 125189.

Kohantorabi, M., Giannakis, S., Moussavi, G., Bensimon, M., Gholami, M.R., Pulgarin, C., 2021a. An innovative, highly stable Ag/ZIF-67@GO nanocomposite with exceptional peroxymonosulfate (PMS) activation efficacy, for the destruction of chemical and microbiological contaminants under visible light. J. Hazard. Mater. 413, 125308.

Kohantorabi, M., Moussavi, G., Giannakis, S., 2021b. A review of the innovations in metal- and carbon-based catalysts explored for heterogeneous peroxymonosulfate (PMS) activation, with focus on radical vs. non-radical degradation pathways of organic contaminants. Chem. Eng. J. 411, 127957.

Li, J., Li, Y., Li, S., Zhu, M., Zhang, J., Li, Y., et al., 2020. Zinc interstitial and oxygen vacancy mediated high curie-temperature ferromagnetism in Ag-doped ZnO. Ceram. Int. 46, 18639–18647.
Li, D., Zhang, X., Zhang, W., 2021. Designing a new reaction system by stacking use of Ti mesh supported Ag/N-TiO2 nano-sheets for enhanced photocatalytic degradation of bisphenol a. Chem. Eng. J. 405, 126867.
Liang, C., Wang, Z.-S., Mohanty, N., 2006. Influences of carbonate and chloride ions on persulfate oxidation of trichloroethylene at 20 °C. Sci. Total Environ. 370, 271–277.
Liu, G., Zhou, Y., Teng, J., Zhang, J., You, S., 2018. Visible-light-driven photocatalytic activation of peroxymonosulfate by Cu2(OH)PO4 for effective decontamination. Chemosphere 201, 197–205.
Liu, N., Ming, J., Sharma, A., Sun, X., Kawazoe, N., Chen, G., et al., 2021. Sustainable photocatalytic disinfection of four representative pathogenic bacteria isolated from real water environment by immobilized TiO2-based composite and its mechanism. Chem. Eng. J. 426, 131217.
López-Vinent, N., Cruz-Alcalde, A., Moussavi, G., del Castillo, Gonzalez I., Hernandez Lehmann, A., Giménez, J., et al., 2022. Improving ferrate disinfection and decontamination performance at neutral pH by activating peroxymonosulfate under solar light. Chem. Eng. J. 450, 137904.
Lu, G., Bernasek, S.L., Schwartz, J., 2000. Oxidation of a polycrystalline titanium surface by oxygen and water. Surf. Sci. 458, 80–90.
Marjanovic, M., Giannakis, S., Grandjean, D., de Alencastro, L.F., Pulgarin, C., 2018. Effect of μM Fe addition, mild heat and solar UV on sulfate radical-mediated inactivation of bacteria, viruses, and micropollutant degradation in water. Water Res. 140, 220–231.
Ni, W., Wu, S., Ren, Q., 2012. Preparation and characterization of silanized TiO2 nanoparticles and their application in toner. Ind. Eng. Chem. Res. 51, 13157–13163.
Oh, W.-D., Dong, Z., Lim, T.-T., 2016. Generation of sulfate radical through heterogeneous catalysis for organic contaminants removal: current development, challenges and prospects. Appl. Catal. B Environ. 194, 169–201.
Ozores Diez, P., Giannakis, S., Rodríguez-Chueca, J., Wang, D., Quilty, B., Devery, R., et al., 2020. Enhancing solar disinfection (SODIS) with the photo-Fenton or the Fe2+/peroxymonosulfate-activation process in large-scale plastic bottles leads to toxicologically safe drinking water. Water Res. 186, 116387.
Prabhu, S., Poulose, E.K., 2012. Silver nanoparticles: mechanism of antimicrobial action, synthesis, medical applications, and toxicity effects. Int. Nano Lett. 2, 32.
Qi, F., Chu, W., Xu, B., 2014. Modeling the heterogeneous peroxymonosulfate/co-MCM41 process for the degradation of caffeine and the study of influence of cobalt sources. Chem. Eng. J. 235, 10–18.
Rodríguez-Chueca, J., Giannakis, S., Marjanovic, M., Kohantorabi, M., Gholami, M.R., Grandjean, D., et al., 2019. Solar-assisted bacterial disinfection and removal of contaminants of emerging concern by Fe2+−activated HSO5- vs. S2O82- in drinking water. Appl. Catal. B Environ. 248, 62–72.
Sang, J., Aisawa, S., Miura, K., Hirahara, H., Jan, O., Jozef, P., et al., 2017. Adhesion of carbon steel and natural rubber by functionalized silane coupling agents. Int. J. Adhes. Adhes. 72, 70–74.
Sayılkan, F., Asiltürk, M., Kiraz, N., Burunkaya, E., Arpaç, E., Sayılkan, H., 2009. Photocatalytic antibacterial performance of Sn4+-doped TiO2 thin films on glass substrate. J. Hazard. Mater. 162, 1309–1316.
Srinivasan, S.S., Wade, J., Stefanakos, E.K., Goswami, Y., 2006. Synergistic effects of sulfation and co-doping on the visible light photocatalysis of TiO2. J. Alloys Compd. 424, 322–326.
Thomas, M.A., Sun, W.W., Cui, J.B., 2012. Mechanism of Ag doping in ZnO nanowires by electrodeposition: experimental and theoretical insights. J. Phys. Chem. C 116, 6383–6391.
Wang, X., Lim, T.-T., 2013. Highly efficient and stable Ag–AgBr/TiO2 composites for destruction of Escherichia coli under visible light irradiation. Water Res. 47, 4148–4158.
Wang, D., Zhou, Z.-H., Yang, H., Shen, K.-B., Huang, Y., Shen, S., 2012. Preparation of TiO2 loaded with crystalline nano Ag by a one-step low-temperature hydrothermal method. J. Mater. Chem. 22, 16306–16311.
Wang, Y., Sun, H., Ang, H.M., Tadé, M.O., Wang, S., 2014. Magnetic Fe3O4/carbon sphere/cobalt composites for catalytic oxidation of phenol solutions with sulfate radicals. Chem. Eng. J. 245, 1–9.
Wang, Y., Zhao, X., Cao, D., Wang, Y., Zhu, Y., 2017. Peroxymonosulfate enhanced visible light photocatalytic degradation bisphenol a by single-atom dispersed Ag mesoporous g-C3N4 hybrid. Appl. Catal. B Environ. 211, 79–88.
Wei, F., Li, J.D., Dong, C.C., Bi, Y.J., Han, X.J., 2020. Plasmonic ag decorated graphitic carbon nitride sheets with enhanced visible-light response for photocatalytic water disinfection and organic pollutant removal. Chemosphere 242, 125201.
Wu, F., Huang, H., Xu, T., Lu, W., Li, N., Chen, W., 2017. Visible-light-assisted peroxymonosulfate activation and mechanism for the degradation of pharmaceuticals over pyridyl-functionalized graphitic carbon nitride coordinated with iron phthalocyanine. Appl. Catal. B Environ. 218, 230–239.
Xu, L., Gong, D., Celi, N., Xu, J.J., Zhang, D.Y., Cai, J., 2022. Biohybrid magnetic microrobots for enhanced photocatalytic RhB degradation and *E.coli* inactivation under visible light irradiation. Appl. Surf. Sci. 579, 152165.
Yun, E.-T., Lee, J.H., Kim, J., Park, H.-D., Lee, J., 2018. Identifying the nonradical mechanism in the peroxymonosulfate activation process: singlet oxygenation versus mediated Electron transfer. Environ. Sci. Technol. 52, 7032–7042.
Zan, L., Liu, Z., Zhong, J., Peng, Z., 2004. Organic modification on TiO2 nanoparticles by grafting polymer. J. Mater. Sci. 39, 3261–3264.
Zeng, J., Liu, S., Cai, J., Zhang, L., 2010. TiO2 immobilized in cellulose matrix for photocatalytic degradation of phenol under weak UV light irradiation. J. Phys. Chem. C 114, 7806–7811.
Zhang, C., Li, Y., Wang, C., Zheng, X.Y., 2021. Different inactivation behaviors and mechanisms of representative pathogens (*Escherichia coli* bacteria, human adenoviruses and *Bacillus subtilis* spores) in g-C3N4-based metal-free visible-light-enabled photocatalytic disinfection. Sci. Total Environ. 755, 142588.
Zhang, J., Zhao, X., Wang, Y., Gong, Y., Cao, D., Qiao, M., 2018. Peroxymonosulfate-enhanced visible light photocatalytic degradation of bisphenol A by perylene imide-modified g-C3N4. Appl. Catal. B Environ. 237, 976–985.
Zheng, W., Tang, C., Xie, J., Gui, Y., 2019. Micro-scale effects of nano-SiO_2 modification with silane coupling agents on the cellulose/nano-SiO_2 interface. Nanotechnology 30, 445701.
Zheng, S., Lin, T., Chen, H., Zhang, X., Jiang, F., 2023. Characterization of young biofilm morphology, disinfection byproduct formation potential and toxicity of renewed water supply pipelines by phosphorus release from corroded pipes. Sci. Total Environ. 884, 163813.
Zhou, Y., Jiang, J., Gao, Y., Ma, J., Pang, S.-Y., Li, J., et al., 2015. Activation of peroxymonosulfate by benzoquinone: a novel nonradical oxidation process. Environ. Sci. Technol. 49, 12941–12950.
Zhou, X., Yang, Z., Chen, Y., Feng, H., Yu, J., Tang, J., et al., 2022. Single-atom Ru loaded on layered double hydroxide catalyzes peroxymonosulfate for effective E. coli inactivation via a non-radical pathway: efficiency and mechanism. J. Hazard. Mater. 440, 129720.
Zottola, E.A., Smith, L.B., 1990. The microbiology of foodborne disease outbreaks: an update. J. Food Safe 11, 13–29.